Unterschrift Betreuer

TECHNISCHE UNIVERSITÄT WIEN
Vienna University of Technology

MASTERARBEIT

Electron dynamics and practical magnetometry using Nitrogen-Vacancy defects in diamond

Ausgeführt am Atominstitut
der Technischen Universität Wien

unter der Anleitung von
Prof. Dr. Jörg Schmiedmayer und Dr. Michael Trupke

durch

Georg Wachter

Stranzenberggasse 6/1 1130 Wien

13. Mai 2014 _____

Zusammenfassung

In dieser Diplomarbeit werden Ensemble Nitrogen Vacanys (NV) behandelt. Das NV is eine Störstelle im Diamantgitters. Das Nv hat einige sehr interessante quantenmeachanische Eigenschaften unter anderem bietet es die Möglichkeit seine Spinzuständet optisch auszulesen, was zu einigen besonders interessante Anwendungen im Bereich der Quanten Information und Quanten Technologie führt. In dieser Arbeit wird die Dynamik von Photonen übergängen in NV Centers gemessen. Um einen Überblick über die zeitlichen Effekte im NV zu bekommen. Unter anderem wir die Lebensdauer des angeregten Zustands von NV^- gemessen und die Zeiten der Übergänge zwischen NV^- und NV^0. Anschließend zu diesen Untersuchungen wird die Stärke und Richtung eines magnetischen Feldes mithilfe eines NV Ensembles gemessen und danach mittels eines Hamiltonians die Stärke und Richtung des magnetischen Feldes bestimmt. Die Größe des NV Centers macht es ideal für magnetische Messungen, da es mit nur zwei Gitterplätzen im Diamantgitter sehr klein ist. Gleichzeitig erreicht man ein gutes Verhältnis zwischen Detektor Größe und Sensitivität. In unseren Untersuchungen konnten wir zeigen das NV Ensemble als Magnetfeldsensoren durchaus mit anderen Methoden mithalten können. Im letzten Kapitel wird auf die theoretischen Grundlagen von Rabi Oszillationen und ihre Anwendung im NV eingegangen mit den sich daraus ergebenden zuküftige Anwendungen eingegangen.

Abstract

In this thesis we want to have an look on nitrogen vacancy (NV) ensembles. NV centres are defects in the diamond with many different features. They are nice quantum system to build an optical readable spin systems. This afford a lot of different application in quantum information and quantum technology. In this thesis the dynamics of photon transitions in a NV centre is measured and analysed. In this measurements we have a look on the ionisation processes between NV^- and NV^0 and the live-time of different levels in NV ensembles. An other interesting process is to use NV ensembles for measure strength and direction of magnetic fields under using the quantum mechanical features of the NV. The size of the NV of only two palaces in the diamond grid make it possible to have very good proportion of detector size and sensitivity. In this thesis we build a magnetometer inside our setup and compare the measurements with the Hamiltonian to find out the strength and direction of the field. The last section is more theoretically and discuss Rabi oscillations in a NV system and gave you an outlook what we want to do in the future.

Contents

1 Nitrogen Vacancy

1.1 What are NV centres?

The nitrogen vacancy defect (NV) is one of over 100 known defects in diamonds. The NV consists of two parts a nitrogen atom and a vacancy. The nitrogen and the vacancy each replace a carbon atom [25].

The NV centre has some interesting qualities as a quantum mechanical system [8].

Great feature is the long coherence time of the spin states. That means the NV is a perfect candidate for a simple quantum system. Another big advantage is that a NV doesn't need such a precise wavelength of the lasers because the diamond is a solid body and has phonon bands which broaden the range of possible excitation wavelengths. So if the energy of the laser is greater than the transition energy the electron is pumped into the phonon states and subsequently falls back to the vibrational ground state of the excited electronic state of the NV.

Another big advantage of the phonon side bands is that the excitation wavelength from the laser and the emitted florescence signal of the NV centre have a different value.

An important application of NVs is magnetic field measurement. The simplest way to do this is to use the Zeeman effect,which describes the energy level splitting due to a magnetic field. This effect can be used in the NV centre in a very clever way. You can even measure the field direction (with some constraint). How does that work? One level of the negatively charged NV^- is a metastable level with a life time 10 times longer than the other levels. There is only one possibility to reach this level, namely from the ± 1 degenerate state of the excited state. The splitting of the $m_s = 0$ and the $m_s = \pm 1$ state is about 2.87GHz and thus can be addressed by a microwave. So the frequency of the microwave is swept and at the right frequency a transition between the spin 0 and the ± 1 states is driven. At this position the intensity of the fluorescence decreases, because the electrons are trapped in the metastable state. They are lost for the fluorescence process. So the only things one needs to measure the magnetic field are a laser to drive the fluorescence of the NV centre, a microwave source and a photo detector

In section 4 experiments with microwaves are explained. In figure 1.1 the levels are shown in a schematic way. The ground and the excited state of the NV^- are triplet states. These states are the interesting ones. They are split by a magnetic field and can be driven by a microwave.

1.2 Creation of NV centres?

It is not really difficult to create a NV centre but if you want something special it can become very challenging. There are a lot of ways crate them: As NV centres consist of a vacancy and an adjacent nitrogen atom in the middle of the carbon lattice of diamond, you can either increase the number of vacancies in a nitrogen rich diamond sample or increase the number of nitrogen via direct nitrogen implantation. Vacancies can be easily created by irradiation of the diamond with particles like electrons, neutrons or ions. With the ions the nitrogen can be implanted directly. In all these processes the crystal

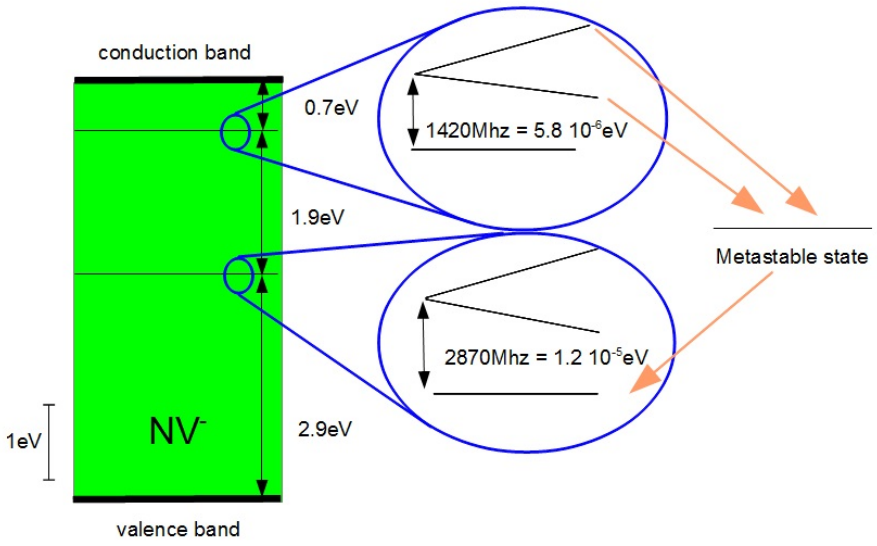

Figure 1.1: Micro waves on NV

grid will be deformed and vacancies are produced. When the diamond is heated up afterwards the vacancies get enough mobility to move towards to the nitrogen. In addition the defects are healed out during the annealing process. The problems lie however always in the detail: irradiation time, energy and angle at which the particles impinge on the diamond. To implement for example a thin layer of NV centres at defined depth or to produc e a single NV at defined position needs specific implantation parameters. Then the charge state of the NV centre also depends on the type of production. That is a big problem and a lot of studies were done in the past. However to our luck a lot of people study these processes and here I had the possibility to use diamond samples which were produced before I started my work on the thesis.

2 Absorption and emission of NV centres

Absorption and emission processes can be easily demonstrated with a free gas of 2-level atoms. There are only two level E_1 and E_2 with a energy difference of δE. Due to finite lifetime τ of the excited state and the Heisenberg uncertainty principle the line width $\delta\mu$ of the emitted photon will be finite, too (see: equation 1)

$$\begin{aligned} \delta E = E_2 - E_1 = \frac{\hbar}{\tau} \\ => \frac{\delta E}{h} = \frac{1}{2\pi\tau} \approx \delta\nu \end{aligned} \tag{1}$$

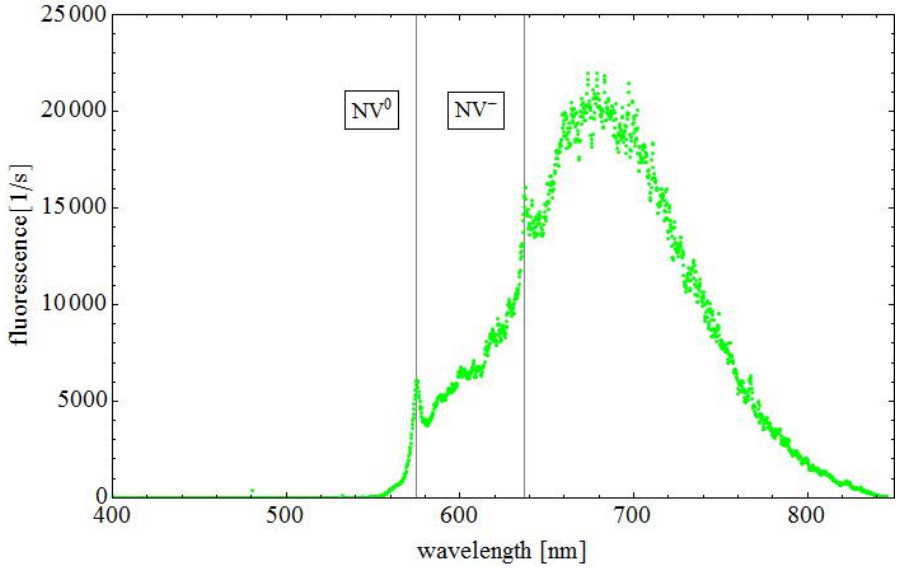

Figure 2.1: NV emission spectrum by induced with green laser light (520nm)

In a solid state system like NV centres in diamond, more processes will occur induced by incoming photons, as e.g. excitation of different phonon modes. In the spectrum both effects will be visible. The sharp lorentzians from the level structure and the phonon side bands from the crystal. These phonon side bands have some disadvantages. At room temperature there is always in the spectrum and is higher than the zero phonon lines. On the other hand this is good because the laser line width doesn't have to be as accurate as in a gas. Some nm more or less is no problem. That means if the energy of the laser is sightly too high electrons go into a phonon side band and fall from there by non radiative processes back to the excited state and subsequently to the ground state.

There are two different charge states of the NV centres: NV^- and NV^0. The different charge creates a different level structure of NV^- and NV^0. So in the NV spectrum shown in figure 2.2 are two phonon lines there and two phonon side bands. It is also possible to drive transitions between NV^- and NV^0 with the right laser wavelength (see: section 3.3.1).

The NV can be classified in four different families. The families differ in the direction of the axis of the NV. Figure 2.3 a diamond grid is shown, the green sphere stands for a vacancy and the red for the nitrogen atom. The axis is defined by the line between the vacancy and the nitrogen atom. It is clear that if the position of the nitrogen is locked there are four possible positions for the vacancy. That is important if the experiment should work with spins and magnetic fields (see: section 4) because the spins are discretized in the axis of the NV. For each family different Zeeman splitting can be observed.

Another nice feature is the metastable state in the NV^- state. This state can only be reached over the ± 1 state of the excited state of the NV^-. The microwave drives

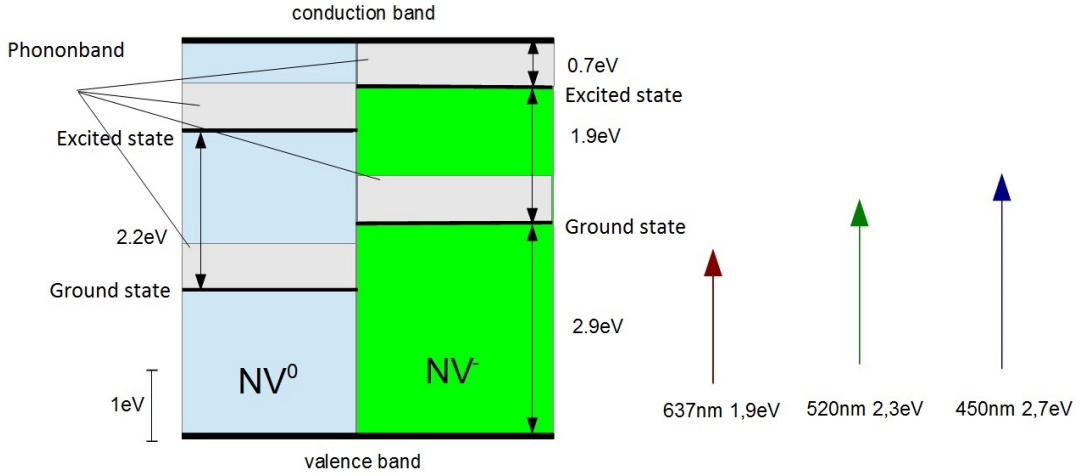

Figure 2.2: NV centre energy levels with different lasers. All levels and lasers are drawn to scale [1]

.

for example the $m_s = 0$ to $m_s = 1$ transition of the ground state and over the green laser the electrons go to the excited state, and from there to the metastable state with a probability of around 50%. With this feature the NV spin state can be read out.

It has to be mentioned that this is all true for single NVs but the experiments in this thesis were done with NV ensembles. These work almost like single NVs but with some small differences. The first difference is clear, there are all 4 families present and not only one. The whole NV signal is larger because there are more emitters. Some more complex differences concern the recombination process (NV^0 to NV^-). However it is noted throughout the thesis if something is different to single NV centres.

In figure 2.2 the energy levels and the lasers which were used in the experiment are shown.

2.1 Green laser light on NV

In the last subsection the NV centres were explained in general. Here I want to talk about the different laser wavelengths in the experiment and their effects on the NV centre. We begin with the green (520nm) laser. In figure 2.4b the fluorescence spectrum for the case that the NV is illuminated with green laser light is shown. The NV^0 phonon line and the NV^- phonon line are clearly visible. So it is possible to bring both NV states to fluoresce with green light. With green light it is also possible to transfer NV^0 to NV^- and also NV^- to NV^0 with a two photon process. How does this transition between NV^0 to NV^- work?
Let's start in the NV^- ground state. NV centre is illuminated with by green light. The electron goes from the ground state to the phonon band and falls back to the excited state. From there the electron can go back to the ground state via a red photon emission

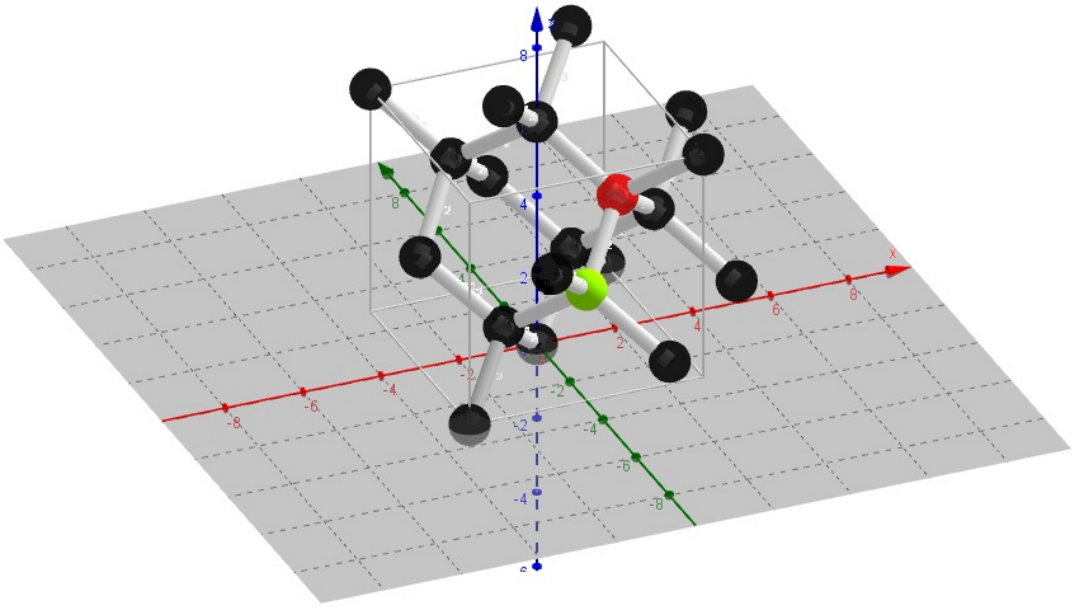

Figure 2.3: Diamond grid with NV. The red sphere represents the nitrogen and the green sphere stands for the position of the vacancy.

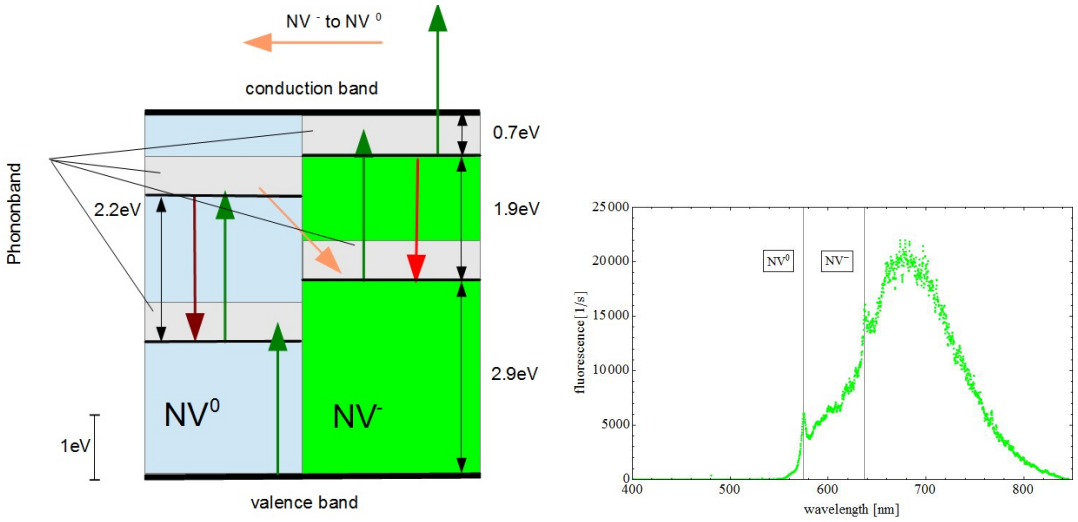

(a) Transitions which can be addressed with the green laser

(b) Green Spectrum

Figure 2.4: Green spectrum with laser light 520nm and energy levels. In the left figure the green arrows stands for the laser, the grey for non-radiative processes, the red for fluorescence, and the orange for charge stage conversion

(>637nm). Another possibility is that the electron is hit a second time and leaves the NV. Now the NV is in the NV^0 state.
In NV^0 the electron can be transferred from the ground state to the excited state and falls back. This process produces the NV^0 zero phonon line (575nm) and phonon sideband. However if the electron is in the first excited state and another electron from the valence band is captured, the defect will change to NV^-.

2.2 Red laser light on NV

Let's begin in the same state as in the last section: the NV^- ground state. The red laser light (637nm) has enough power to transfer the electron to the excited state where it can fall back to the ground state again. This fluorescence line can't be seen in the spectrum because a dichroic mirror is used to filter out the excitation light at the same wavelength. The emission spectrum in figure 2.5b is shown for wavelengths between 650nm and 850nm. The red laser (637nm) is also strong enough to ionize the NV centre ($NV^- -> NV^0$). But it does not bring the NV^0 to fluoresce. So the NV centre will remain in the NV^0 ground state. For single NV centres the story ends here. Whereas for NV ensembles there is also a small possibility to spontaneous get back to NV^-, though this process is not yet well understand. Simplifying one can say that red light pumps NV^- to NV^0.

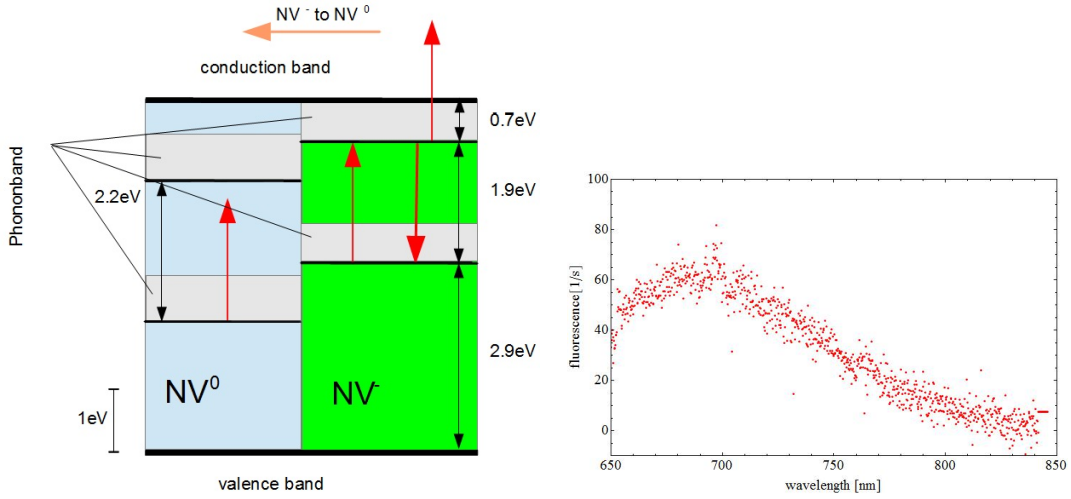

(a) Transitions which can be addressed with red

(b) fluorescence signal for red illumination

Figure 2.5: Energy levels and Red Spectrum for red (637nm) excitation. The red arrows up stands for the red laser light, the red down for the fluorescence, the grey for non-radiative transitions and the orange one for charge stage change.

2.3 Blue laser light on NV

The blue laser light of 450nm brings only NV^0 to fluoresce and pumps in both directions. But in contrast to red light the blue light has enough energy to transfer the electron directly from the ground level of NV^- to the conduction band (no NV^- fluorescence) and transfers in that way NV^- to NV^0. This is a very fast process because it is a one photon process. Due to the fact that the NV^- to NV^0 transition is faster than the NV^0 to NV^- process, the NV centre is going to stay most of the time in the NV^0 state [1].

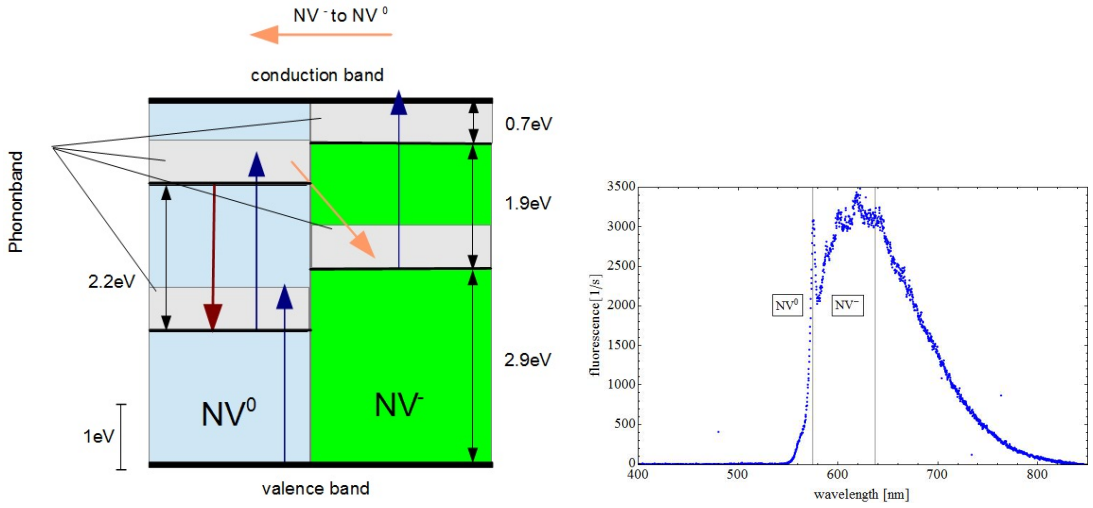

(a) Transitions which can be addressed with blue laser

(b) NV fluorescence induced by blue laser light (450nm)

Figure 2.6: Energy levels and the emission spectrum for blue laser excitation.

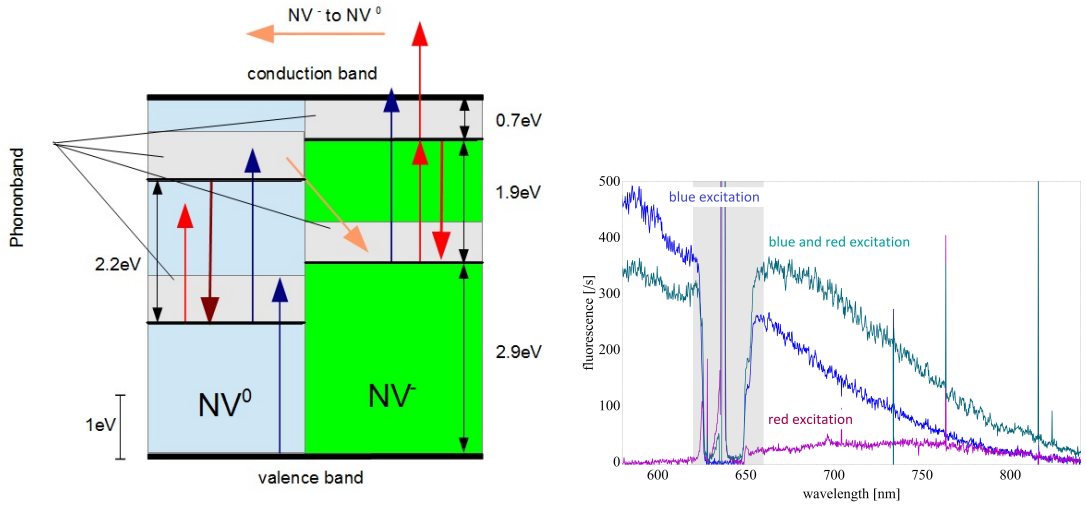

(a) Transitions which can be addressed with blue (450nm) and red (637nm) laser light

(b) Emission spectrum of only blue, only red and red+blue excitation. The spectrum of the gray area is filtered out by a notch filter. The remaining lines in the filtered area come from the red laser which is not filtered out completely.

Figure 2.7: Energy levels and emission spectrum for simultaneous blue and red laser excitation

2.4 Red and blue on NV

Very interesting things happen when NV centres are illuminated with red and blue light simultaneously. Both, the blue and the red laser light will transfer the NV centre to NV^0 but at 450nm the recombination process to NV^- will also take place and will keep the charge state transfer going. So it is possible to set the NV in an initial state by choosing the right relation between blue and red laser intensity.

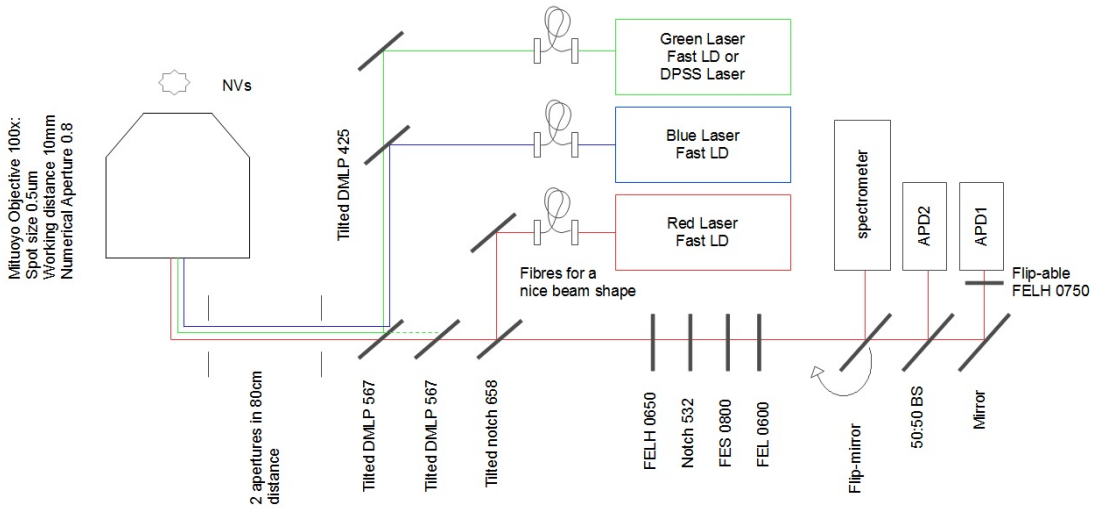

Figure 3.1: Scheme of the experimental setup. The laser light is produced by some laser diodes and a DPSS laser. For a good beam shape each of the laser is coupled through a fibre. After the fibres all lasers have a nice gaussian beam shape. All laser colours are coupled in to the main path by means of dichroic mirror filters. To be sure that all beams are aligned on the same path two apertures are build in. The filters are used to discriminate the NV emission signal from excitation light, scattering and background. Only incoming light between 600nm and 800nm pass the filters.

3 Temporal features of the luminescence NV centre

For a magnetic measurement with NV centre it is essential to know what happens with the NV in time because there may be effects which induce charge state conversion which are different in pulsing and continuous operations.
At first I will explain the experimental setup and measurement procedure. Then the diode lasers are characterised and their rising and falling time are measured. Afterwards the lasers are used to excite the NV centre and induce charge state conversion to measure the lifetime of excited state of NV^-, the duration of the ionisation process from NV^- to NV^0 and the recombination process from NV^- to NV^0.

3.1 Schematic view of the experiment

In the course of the diploma thesis three PC controllable lasers (including pulse mode) were integrated into the experiment. The different colours of these lasers are green at 520nm (50mW), red at 637nm (150mW) and blue at 450nm (100mW). Each one of these lasers is coupled separately into a fibre to get a nice beam shape. This is important for the objective which only can produce a nice and small light point if the beam shape is very good. The beam comes from above and goes throw an objective. The diamond is located under the objective on a translation stage. This design is ideal to scan different areas of the diamond such as different NV densities or single NVs.

Also a green DPSS Laser with 500mW is integrated in the setup because sometimes higher powers are convenient.

It is very important to align all lasers at the same point on the diamond because all lasers must see the same NV centres. From the diamond itself two signals are emitted: the reflection signal from the surface and the interesting fluorescence signal from the NV centre. So these two signals go back through the objective and are guided to the filters. The first filters cut out all laser lines, two additional filters block wavelengths over 800nm and under 400nm to reduce the background. Sometimes neutral density filters are used to reduce the signal because the response of the APDs (Avalanche Photo Diode) is not linear for higher count rates than $\approx 1 Mcts/s$. They are needed because the signal of a single NV is some orders magnitude smaller than from NV ensembles.
After all these filters the background and fluorescence signals go into a blue box which contains two APDs and the spectrometer input. The dark box serves as shield against additional light from the environment because the APDs are able to count single photons. To measure the signal originating only from the NV centres, it is necessary to always make an additional background measurement on a diamond area without any NV centres and then subtracting it from the measurement.

The signal from the APDs goes to a time tagger which marks every photon with a time stamp. The time tagger sends the channel input number and the time stamp to the computer. Also every trigger signal for the lasers gets to the time tagger and gets a time stamp.

In this way the histogram program on the computer can discriminate between the different input channels (triggers and APDs). In a histogram program the whole data is analysed and plotted. In this manner all pulse processes are controlled and analysed via the computer.

3.2 Laser characteristics

The lasers are current switched diode lasers. We used the chip IC-HG from IC-Haus. This laser driver chip is able to switch up to 3A with 200MHz and has rising and falling times in the range of 1ns. From the electrical point of view these are amazing numbers for a driver chip. This chip is controlled by a high speed digital logic signal. A very fast emitter coupled logic (ECL) produces the fast pulses and controls the switching process of the laser (see appendix A for more information).

The lasers have four different operation states, the first two are easy: continuous waveform (CW) and OFF. In the CW state the lasers are driven continuously and not in a pulsed way. The next modus is the TTL (Transistor Transistor Logic stands for the digital communication technologies): here it is possible to switch the lasers using a TTL signal, the shortest pulse length is 100ns. The last modus is the pulsed modus: In this case the TTL pulse serves only as trigger and an internal logic produce pulses in the range of 2ns - 10ns. The short pulses are used to study the lifetime of the excited states of NV^- and NV^0.

The laser diodes which are used for the pulsed operations are built without any crystal for frequency doubling. This is very important because the time needed to switch the

diode name	wavelength	power	falltime TTL	falltime ns pulse
LD-520-50SG	520nm	50mW	0.6ns	0.32ns
LD-450-100SG	450nm	100mW	13ns	2.9ns
HL63133DG	637nm	170mW	9.8ns	1.8ns

Table 1: summary over all laser diodes which are integrated in the lasers in the experiment.

diode name	wavelength	problem
ADL-63302TL	638nm	peakform in TTL mode was not a rectangle. Massive overshoot at the beginning of the pulse (350%)
DJ532-40	532nm	switching time in the range of 100ns

Table 2: Laser diodes which were tested but not convenient for pulsed laser operations.

laser diode depends only on the electronic semiconductor characteristics of the laser diode. In the specification sheet for the green and the blue laser the manufacturer guarantees a modulation frequency over 100Mhz. This is a very careful specification. 100Mhz modulation are possible in all states of operations. It is possible to reach a pulse length down to 2ns, but only if you decide that you don't need the full power and a Gaussian pulse form is enough for your purposes.

The red laser light (637nm) is produced by the laser diode HL63133DG. This laser diode is not specified for pulsed operations by the manufacturer but the diode still switches fast enough. In the figure 3.2 the falling time is around 10ns, that's 5 times more than the blue and green laser. In this thesis the red short pulses are not needed.

The green laser light is produced by the laser diode LD-520-50SG. This diode is optimised for pulsed operations, has a wavelength of 520nm and a power of 50mW.

The blue laser light (450nm) is produced by the laser diode LD-450-100SG. This diode is also built for pulsed operations and has a maximal power of 100mW.

The intensity of the laser diodes are controlled by an internal analog signal in the laser driver. The laser intensity can be set manually or remote via the PC.

Table 1 is a summary over these laser diodes and table 2 shows laser diodes which were tested but not convenient for pulsed operations.

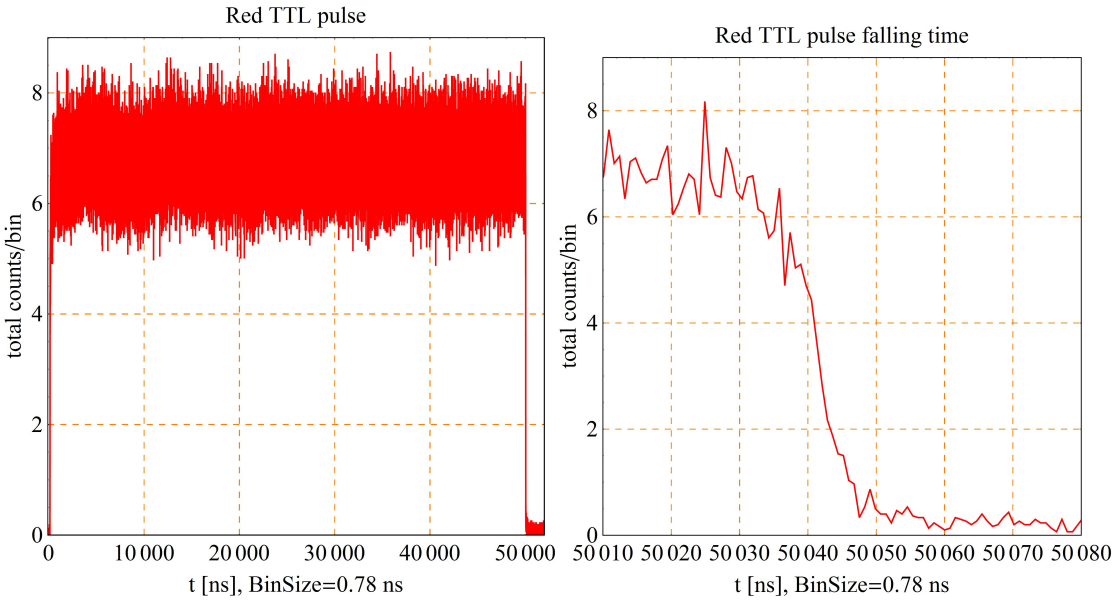

(a) Red TTL pulse

(b) Zoom into the falling time of the red TTL pulse

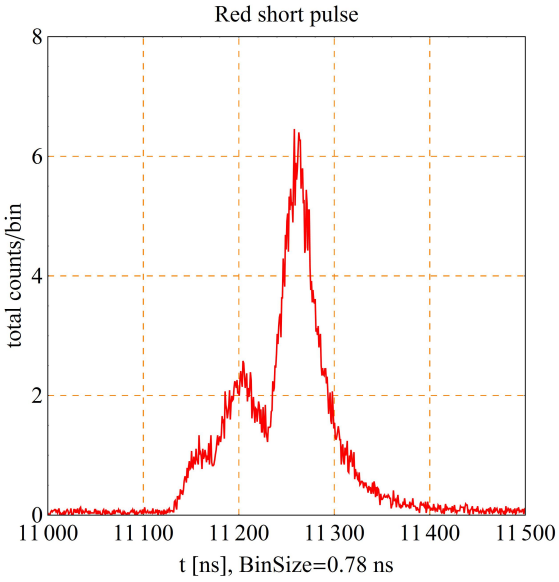

(c) Red short ns-pulse

Figure 3.2: Red pulsed laser characteristics.

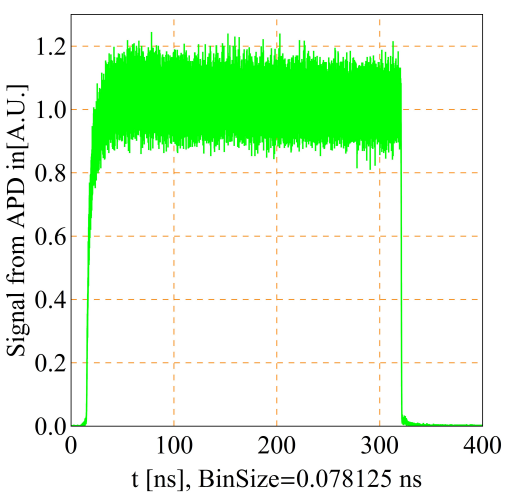

(a) Green TTL pulse

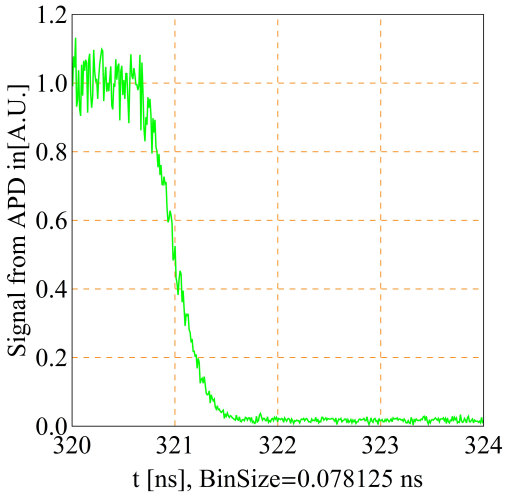

(b) Zoom into the falling time of the green TTL pulse

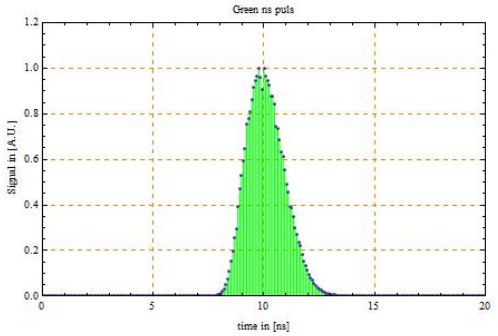

(c) Green ns pulse

Figure 3.3: Green laser characteristics. The performance of the green laser is very good. The green laser was the first laser that was built with the pulsed modus.

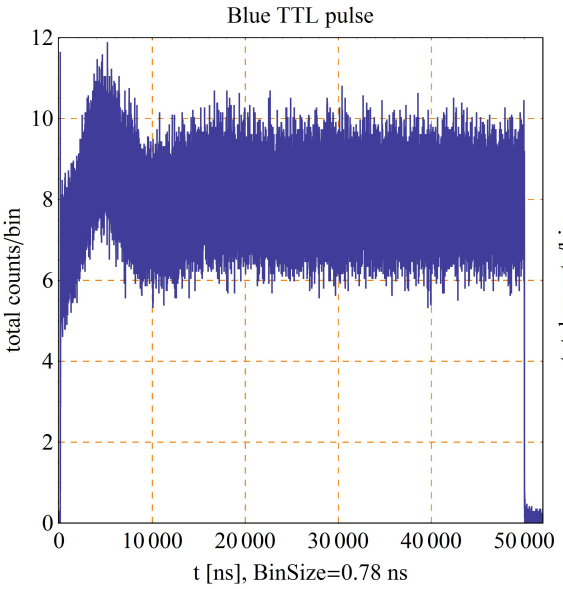

(a) Blue TTL pulse

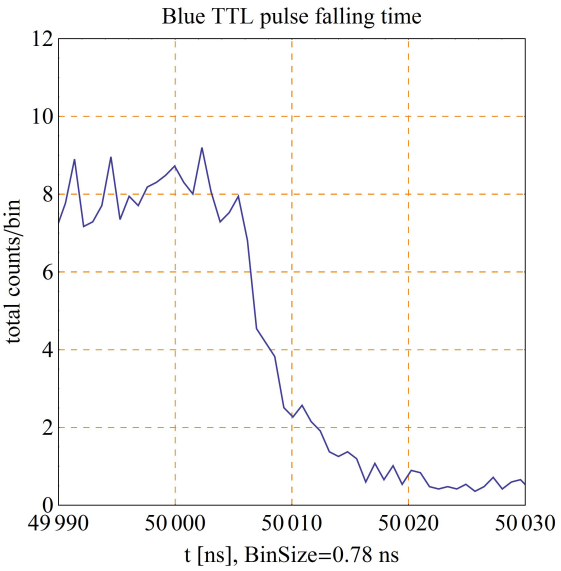

(b) Zoom into the falling time of th blue TTL pulse

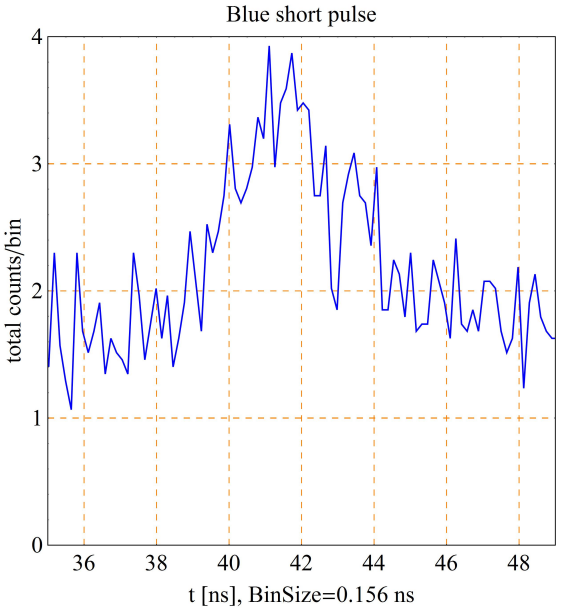

(c) blue ns pulse

Figure 3.4: Blue pulsed laser characteristics

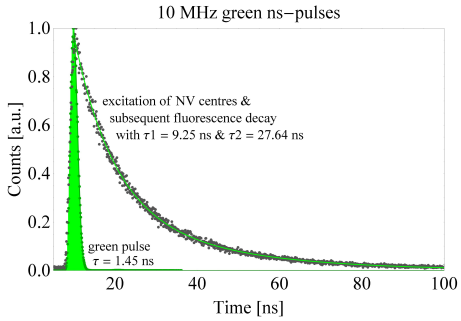

Figure 3.5: Green ns pulse on NV. The green area shows only the laser. This measurement is made with a repetition rate of about 10Mhz. The fit signal is a sum of two $a * e^{\frac{-t}{\tau}}$ functions.

3.3 NV centre excitation via laser pulses

3.3.1 Short green pulse

In this subsection the life time from the first exited state of NV^- is measured. For this reason the green pulsed laser is set to the short pulse mode. Just as a remember green light brings NV^0 and NV^- to fluoresce. So we expect two different falling times. Other experiments on single NVs say that the life time should be in the range of 12ns for NV^- and 21ns for NV^0 [19]. But these values vary for each NV because of the stress at the position of the single NV [3]. Our measurements suggests a double exponential fit with $\tau_1 = 9ns$ and $\tau_2 = 28ns$ (see figure 3.5). It is difficult to assign these times to an individual NV centre because we don't discriminate between $m_s \pm 1$ and m_s 0 states [5]. In addition we block with the filters a big amount of all fluorescence from NV^0.

3.3.2 Red and green laser light on NV centre

In these measurements we look at different pumping times for green and red laser light. At the beginning all laser intensities were set in that manner that the NV fluorescence for each laser is similar. So if the NV is illuminated with a red or green laser a similar number of ticks is counted. The problem from this calibration is that the red light brings only NV^- to fluoresce, but pumps it simultaneously to NV^0. There are only few NVs which are in the NV^- state and produce light. That means that the red laser has a high intensity and the green laser has a very low intensity. But the big advantage is that the features of the two lasers are shown very well. In figure 3.6 the two lasers are shown. The intensity values are not changed in all the following measurements.

A pulse train was constructed with a green and a red laser pulse. What should happen? The green pulse pumps the majority of NVs into the NV^- state. This process is very fast in comparison to the opposite process. The red pulse brings the NV^- to fluorescence. Now we observe a much higher signal when we illuminate the NV centre with red laser pulse because more NV^- states are populated due to the previous green laser pulse. Remember that the fluorescence signal of each laser is the same. The red

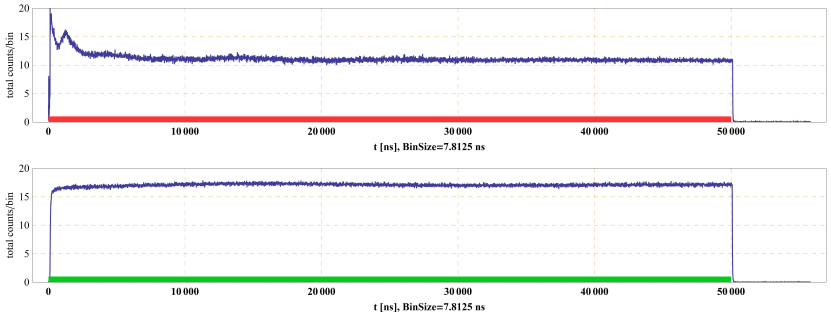

Figure 3.6: In this figure a green and a red laser pulse with $50\mu s$ are shown the intensity of both pulses are set in that way that every pulse produces a similar signal. The features at the beginning of the red pulses happen because this diode is not optimised for pulsed operations.

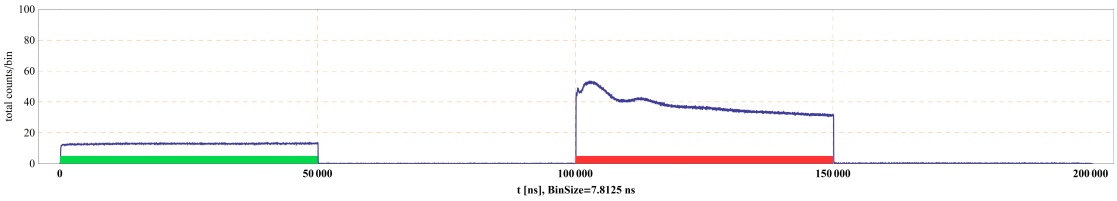

Figure 3.7: In this figure a green and red laser pulse with $50\mu s$ are shown. The red pulse rises by a factor of three compared to only-red excitation.

pulse decreases subsequently because the red light pumps the NV^- to NV^0. In figure 3.7 the pulse train is shown.

It is also very interesting what happens if you use a pulse train of $50\mu s$ pulses one laser colour and the other laser colour is in CW mode. In this measurement the pumping process between NV^- and NV^0 is shown. In figure 3.8 the whole process is shown. In the first case the red laser is switched on the whole time and the green laser is pulsed. Here the pumping effect of the red laser is shown in a very nice way. The green $50\mu s$ pulse pumps the NV centres from NV^0 to NV^-, that is the reason for the curve form during the pulse. After the pulse the red laser light pumps the NV back to the NV^0 state.

In the second case the opposite process is measured. During the 50μs red laser pulse the fluorescence of the NV is higher than in the red pulse alone without green. After this pulse the pumping back to the initial state goes very fast.

3.4 Outlook

The switching off process of the lasers works very well. The switching on process works well for the green laser but for the red and the blue laser some oscillations can be observed. The fast pulses work very well for the green laser, but for the red and blue

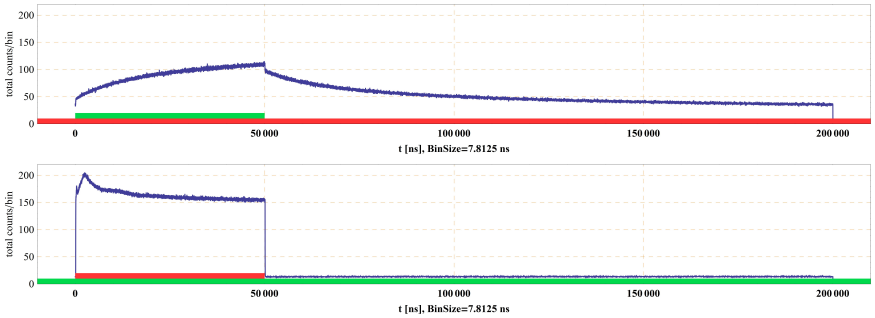

Figure 3.8: In this upper figure a green TTL laser pulse with $50\mu s$ duration and a red laser in the continuous waveform mode are shown. The figure below shows the opposite colour case

laser produce some problems. With these pulsed lasers a lot of interesting analysis of the NV centres are possible. A big variety of time-dependent processes can be studied by means of pulsed excitation. The interesting ones are the Rabi oscillations (see: section 5) because in this system a lot of nice quantum effects can be shown. It is also possible to study the dynamics of the ionisation process in the NV centre.

4 Optically Detected Magnetic Resonance (ODMR) Experiments on NV centre

This section describes the microwave (MW) features of a NV centre. In the first subsection the Hamiltonian which contains the energy splitting of the NV is calculated. In these calculations the field direction is a variable. In the next step the direction of the magnetic field is set in the (0,0,1) and the (0.5,0.5,1) direction, because these directions are realized in the experiment. These vectors are normed and multiplied by the strength of the B-field. In the next subsection the experiment is explained and the data is plotted. In the last subsection the experiment and the theory are compared to each other.

4.1 Theoretical Background

The ground state of the NV^- centre is a triplet state and normally degenerate. It can be split by a magnetic field. The transition between the $m_s = 0$ and the $m_s \pm 1$ state is separated by 2.87GHz and thus can be reached by a microwave.

The Hamiltonian of the NV (ground state) is given by the following formula:

$$\hat{H}_{ges} = \hat{H}_{zfs} + \hat{H}_z + \hat{H}_{hf} \tag{2}$$

- $\hat{H}_{zfs}$ stands for the zero field splitting between the $m_s = 0$ and the $m_s = \pm 1$ states.

- $\hat{H}_Z$ accounts for the Zeeman and Stark effect, the magnetic field dependency of the spectral lines.
- $\hat{H}_{hf}$ gives a solution for the hyperfine splitting.

The experiment was performed on NV ensembles and it was not possible to resolve the hyperfine splitting. This term is neglected in this section. Let's begin with the zero field splitting which is given by:

$$\hat{H}_{zfs} = \frac{1}{\hbar}[D(S_z^2 - \frac{1}{3}\boldsymbol{S}^2) + E(S_x^2 - S_y^2)] \tag{3}$$

D describes the zero field splitting between the $m_s = 0$ and the $m_s \pm 1$ state. E describes the splitting between the $m_s = 1$ and the $m_s = -1$ state due to strain or electric fields. In an ideal NV this term is zero. But stress in the diamond produce this non zero E. In the experiment both are measured to D=2.87 GHz and E=0.0037 GHz. They can be approximated by a dipole interaction. (see [12] for the derivation).

The Zeeman term is given by equation 4 [8].

$$\hat{H}_z = -\gamma_e \hbar \vec{B} S_z \tag{4}$$

If we combine the Hamiltonians to $\hat{H}_{spin} = \hat{H}_{zfs} + \hat{H}_z$ and solve the time independent Schrödinger equation $\hat{H_{spin}}\phi = \epsilon\phi$ with Pauli matrices. We can write:

$$\hat{H}_{spin} = \begin{pmatrix} D-E & -i\gamma_e\hbar B_z & i\gamma_e\hbar B_y \\ i\gamma_e\hbar B_z & D+E & -i\gamma_e\hbar B_x \\ -i\gamma_e\hbar B_y & i\gamma_e\hbar B_x & 0 \end{pmatrix} \tag{5}$$

From equation 5 the eigenvalues are calculated. Typically three eigenvalues are calculated (one for each spin-state 0,1,-1).

$$f_i(\boldsymbol{B}, D, E) = Eigenvalues(\hat{H}_{spin}(\boldsymbol{B}, D, E)) \tag{6}$$

Equation 6 is a very big and long mathematical term but it is an analytical solution. This function is calculated by means of the program mathematica 8. So there are three eigenvalues which depend on a magnetic field B and the values of E and D.

The magnetic field B is given in the basis of the NV centre, and there are four families of NVs (see figure 4.1). Each family has a different coordinate system. So there are three eigenvalues times four families, which leads to 12 different energy levels. The good point is that there are no transitions between the families. In the experiment two directions were used: (0,0,1) and (0.5,0.5,1). For (0,0,1) there is only a field in the B_z direction. In figure 4.1 the axis of the NV is shown. In the next step the field coordinates will be projected onto the axis of the four NV families. You can see that the projections of the magnetic field are in all four cases the same for the (0,0,1) direction. So it can be expected that there are two big visible peaks in the measurement. That means that the eigenvalues for all families of the NV are the same. So it is good to start in the experiment with this direction because here the contrast is maximized.

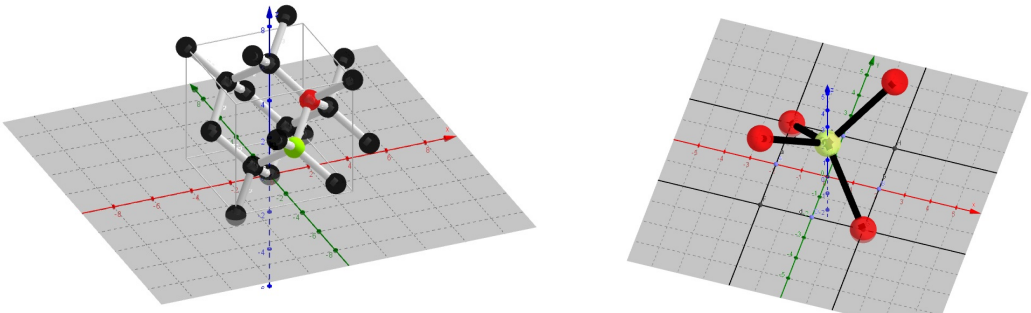

(a) (b)

Figure 4.1: This is a schematic figure of a NV. The green sphere represents the nitrogen atom and the red spheres are the possible positions of the vacancy. The diamond cubic crystal structure can be described by two fcc (face centred cubic) Bravair lattices which are shifted by $\frac{1}{4}$ of the body diagonal. The vectors of the vacancys are space diagonals (1 1 1), (-1 -1 1), (-1,1,-1) and (1,-1,-1).

Figure 4.2 shows an example for eigenvalues which depend on a magnetic field. The magnetic field is 10 times bigger than in the experiment, so that the whole effect is shown.

In figure 1.1 the Zeeman splitting of the states is shown. Between the three levels of the ground state there exist two possible transitions for single photon processes according to the spin selection rules. Two photon processes will be neglected. The excited state has also three levels which can be split by the Zeeman effect. The NV centre also has a metastable state. Only transitions from the ± 1 state are allowed to reach the metastable state. However only if the right frequency drives the three level ground state and an excitation to the ± 1 excited state is performed, the electron stays some more hundreds of ns in the metastable state. In this case the intensity will decrease.

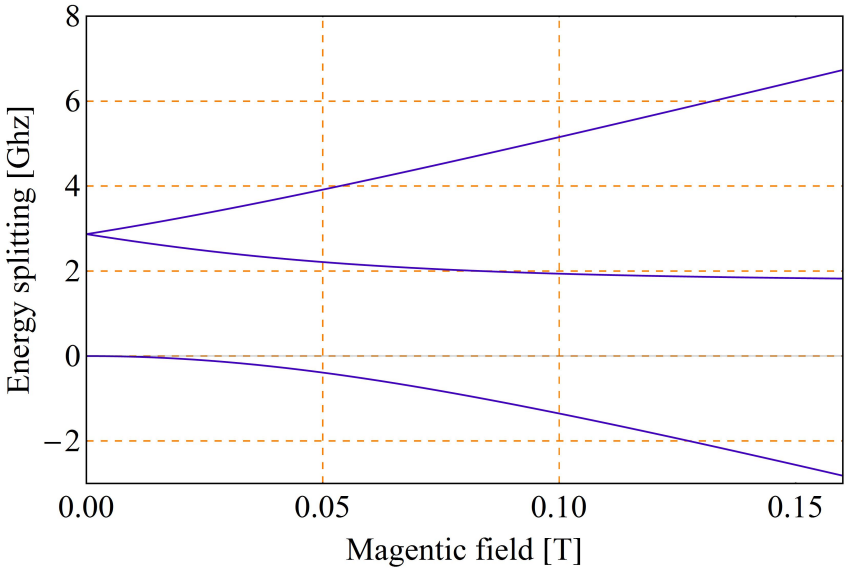

Figure 4.2: Calculated eigenvalues for a magnetic field between 0 and 160 Gauss and E=0.0005 with a direction of (0,0,1).

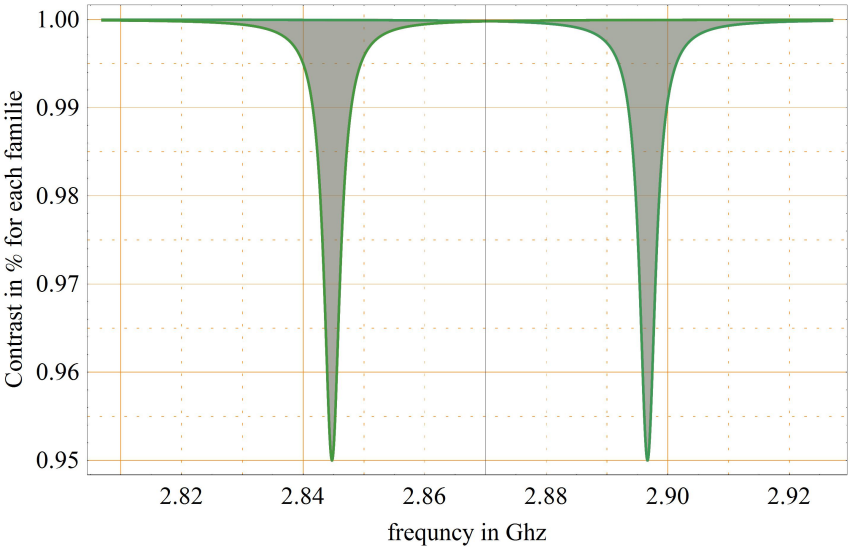

Figure 4.3: ODMR Calculation with a magnetic field of 16 Gauss pointing in the direction of (0,0,1). For this plot only the frequency of the peaks is calculated, the width and the depth are chosen to be in the same order of magnitude as in the experiment.

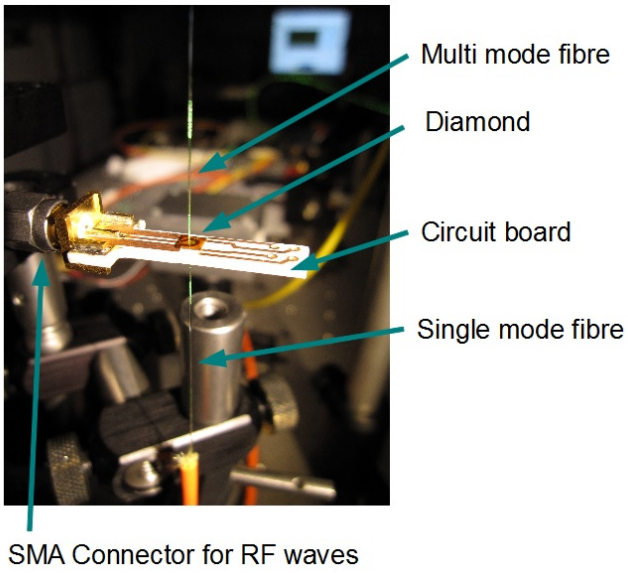

Figure 4.4: Photograph of the fibre on the diamond

4.2 Experimental setup for ODMR measurement

Apart from the setup with the objective which is described in section 3.1 some experiments were performed on a fibre setup. First I will illustrate the fibre setup, compare both setups, and then I will show the results of the measurements.

In figure 4.4 shows the heart of the experimental setup. This experiment is named fibre setup because it works with a fibre instead of an objective.

The figure 4.5 shows how the laser light is produced in the experiment. This light comes from a $532nm \pm 1nm$ DPSS Laser (green) and the laser intensity is stabilized by a PID regulator. For other application also a red diode laser is integrated in the setup.

Both lasers are coupled to a single mode fibre, which guides the light to the diamond. The fibre comes from the top and is held by a Thorlabs-mount which is mounted on a mini stage for positioning the fibre before and during the glueing process.

The diamond is on top of a circuit board with an antenna. In the circuit board is a bore hole and through this bore hole a multimode fibre guides light to the sensor system. The photo diode is situated after some filters to cut off the green laser and the NV^0 signal. So the sensor will mostly see the NV^- signal.

The frequency (RF) circuit guides the microwave to the antenna. The frequency generator (TTi TGR6000) produces the microwave. The next step is done by the MW amplifier (Minicircuits ZHL-16W-43-S+), which amplifies the signal to about $+45dBm$. From the amplifier another line guides the signal to the antenna. The antenna is built as a short between ground and signal to maximise the current flow through the antenna to get a maximised magnetic field (see equation 5). In appendix D a short overview is shown of how to build a HF antenna.

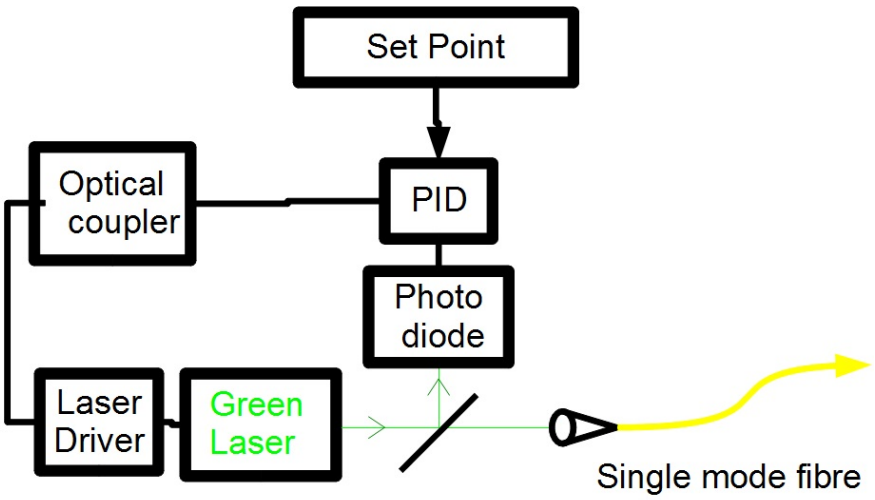

Figure 4.5: Simplified schematic view of the laser stabilisation. The laser light has a wavelength of about $532 \pm 1nm$. The laser light is split in two parts. One of them is guided to a single mode fibre and the other one is send to an photo diode. The signal for the photo diode goes to the PID controller. The PID controller can change the laser intensity over a optocoupler and the laser driver. In that way the controller stabilised the laser intensity.

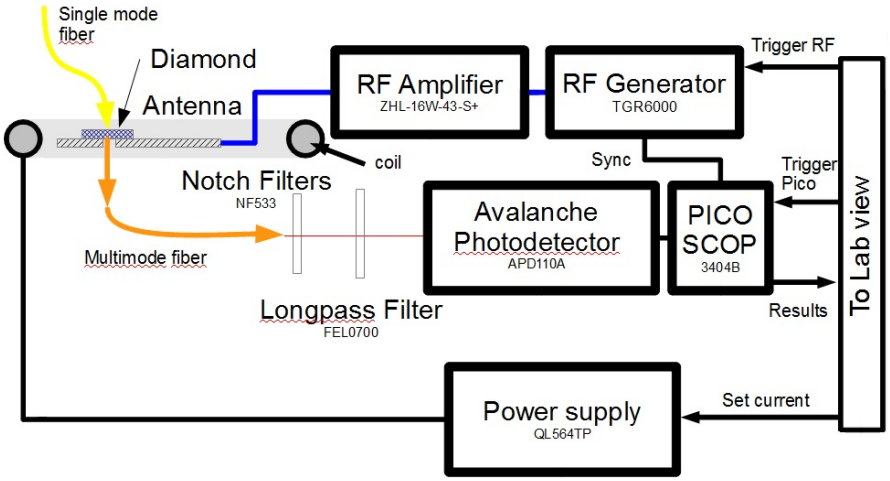

Figure 4.6: The labview program is the main control unit. Over the trigger labview sets the measurement points. Over the trigger RF the MW generator starts to switch the frequency. Two lines are measured, the Sync Signal from the MW generator and the avalanche photon detector signal.

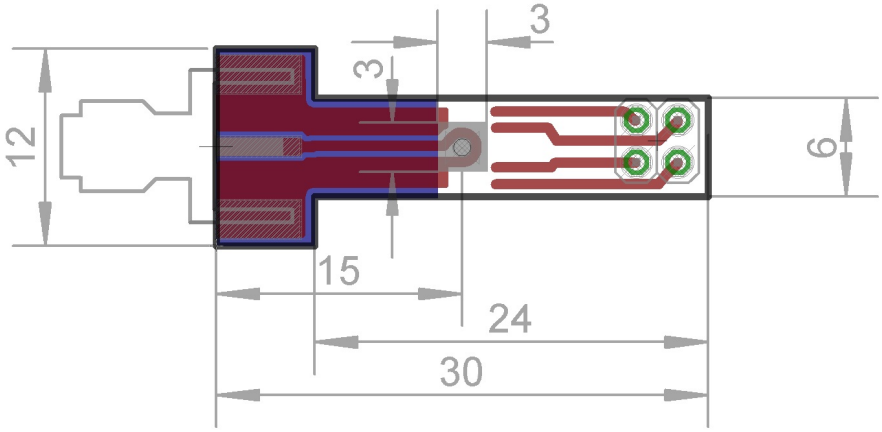

Figure 4.7: Here the MW antenna is shown. Red is the top copper layer and blue is the bottom. The antenna is build out of 2,5mm thick ceramic board, the four lines on the right side are for future applications (maybe Structures on diamond). Ever dimensions in mm

In general one aims for a high power of the MW wave, but in reality values like 16W implies also some trouble: First the microwave heats up the diamond. In one experiment the glue which holds the diamond on the circuit board was burned away. This glue starts melting at temperature over 250°C. In the end there is only need for 1W (30dBm at the antenna) output power form the MW amplifier. The contrast does not reach its maximum value but the setup does not glow.

All around the antenna a coil was mounted to produce the magnetic field. The current through the coils is controlled by a remote power supply (name: QL564TP). In that way the coil can create a field between 0 and 16 Gauss at the position of the diamond. The coil has a radius of 15cm and consists of 50 turns. Compared to the diameter of the multi-mode fibre with $50\mu m$ the coil is much bigger and ensures a homogeneous magnetic field in strength and direction.

The sensor (Thorlabs APD110A) is read out by a picoscope , a computer controlled oscilloscope (Pico Technology 3404B). It reads out 2 million points in a time of 25s to get good statistics. In this time the frequency generator steps through a list of frequencies and levels: first the desired frequency value is set and the fluorescence is counted in the next 25ms. Afterwards the frequency generator is turned off to count the fluorescence without a microwave. Then these two signals will be divided to get the contrast. In that way one is less sensitive to fluctuations of the laser intensity.

The next problem is mechanical vibration. The solution is to measure fast enough in this experiment: 25ms with MW and 25ms without RF. So the setup only has to be stable within 50ms. With all these techniques it is possible to get nice a signal. One example is shown in figure 4.8.

In the next step a current flows through the coil and generates a magnetic field. Measurement with a Hall-sensor shows that the field at the position of the diamond has

a strength of approximately 16 Gauss (or 0.0016 Tesla) for a current of 4A in the coil.

Here I want to compare the fibre setup and the microscope setup. Both have advantages and disadvantages. The advantages of the fibre setup are:

- There is no need to have an expensive objective and a 3D piezo stage. You don't have to align the laser light through the objective and find the focus. The only thing you have to do is to couple the laser light into a fibre. These are very nice features.
- The system is very small. This is good because it is possible to bring the whole system inside a bath cryostat.

On the other side there are some other disadvantages.

- There is no possibility to scan the whole diamond. Only the area where the fibre is glued will be illuminated by the laser light.
- The experiment works only with NV ensembles because the sensor only looks at the position where the fibre was glued.
- Low collection efficiency because there are no optics between diamond and fibre.
- It isn't so easy to glue fibres There are a lot of possible mechanical problems. The first one is the positioning of the fibres. That is done over two mini stages (Thorlabs DT12XYZ/M). Just before the gluing procedure the system is held at three points: the circuit board and two fibres. That's not ideal for the gluing process because if for example the circuit board swings a little bit and the fibres don't, the gluing points in are motion. It works for one fibre if this fibre is pressed onto the diamond. But for two fibres it gets quite problematic. In the end the circuit board and the fibre stages were all mounted onto one steel mount. That reduces the oscillations a little bit.

In my measurements I want to look at the electromagnetic features of NV ensembles. The fibre setup is ideal for this study.

In figure 4.9 a measurement without a magnetic field is shown. The reason why it is not only one peak lies in some other effects, first stress in the diamond, then the earth's magnetic field and maybe influence from the environment. There is no shield against E or B fields.

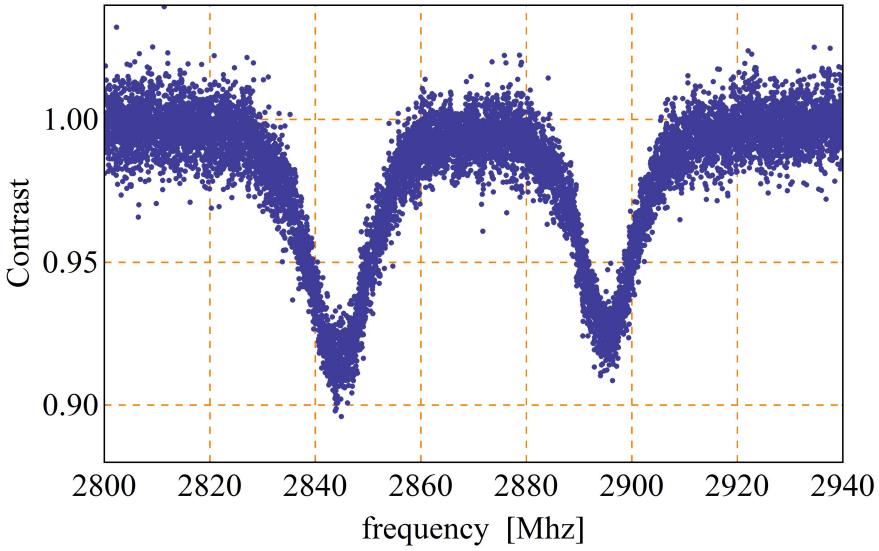

Figure 4.8: ODMR measurement with a magnetic field of 16 Gauss in the (0,0,1) direction.

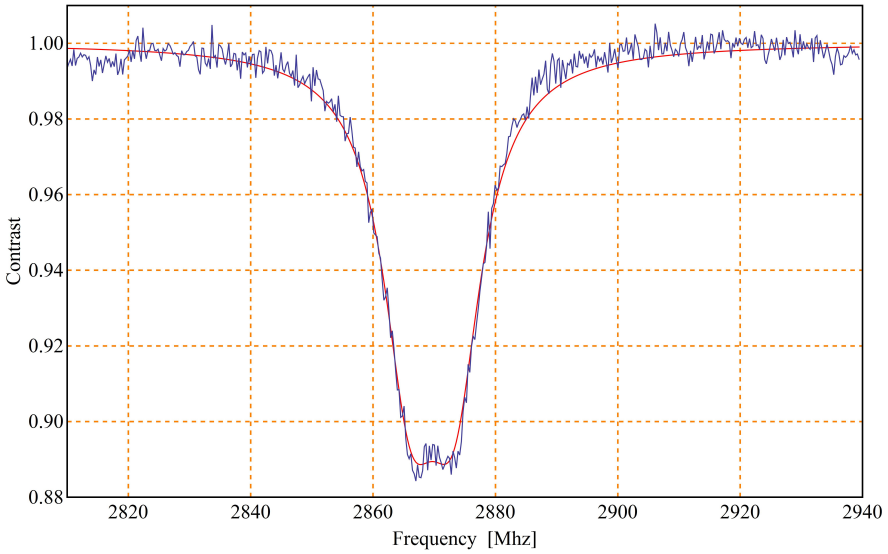

Figure 4.9: ODMR measurements without a magnetic field. The reason why still two peaks are visible instead of one is due to the earth's magnetic field and stress in the diamond.

4.3 Results

In this section the theory (see section 4.1) and the measurements (see section 4.2) are compared to each other. In section 4.1 only the frequency of the transitions are calculated. The width and the depth for the lorentzian curves are set so that it is possible to compare the theory and the measurement.

4.3.1 Results for a magnetic field direction of (0 0 1)

In the first figure 4.10 the measurement with a magnetic field in the direction of (0,0,1) is shown. Each of the four families produce two peaks. The field direction is chosen such that all eight peaks degenerate to two peaks. In this field configuration the biggest signal is expected.

The experimental data was analysed with a fit (see: equation 7). This fit function $f(x)$ is built for a general case. For the magnetic field direction (0,0,1) only two lorentzians are needed.

$$f(x) = \sum_{i=1}^{4} \left(1 - \frac{a}{1 + \frac{(-w_i(\boldsymbol{B}) + x_0 + x)^2}{g}} - \frac{a}{1 + \frac{(+w_i(\boldsymbol{B}) + x_0 + x)^2}{g}} \right) \tag{7}$$

So x_0 is the position between the two peaks and this value is the same for all small B fields. For big magnetic fields (see figure 4.2) asymmetries occur. The picture shows the energy splitting between 0 and 160 Gauss. This fit function only works well, with a magnetic field in the range of 0 to 16 Gauss as used in our experiment.

For big magnetic fields x_0 also depends from the magnetic field. The width of the peaks is described by g. It is important that this parameter is set to the same value for all strengths of the magnetic field. This distance between the peaks is described by the variable w_i. This variable is the only one which depends on the magnetic field.

To compare experiment and model some parameters for the model are need. We set D to 2.87 GHz and E to 0.0037 GHz. There is also a possibility to built an offset for the magnetic field this inside the equation. This offset is set to zero.

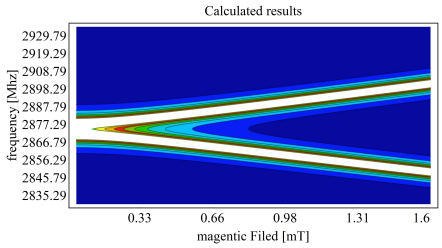

(a) Energy splitting (model)

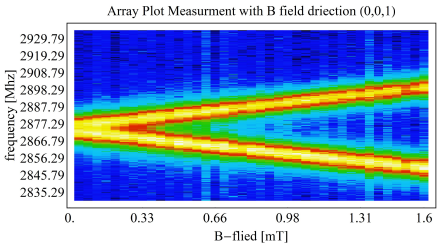

(b) Energy splitting (experiment)

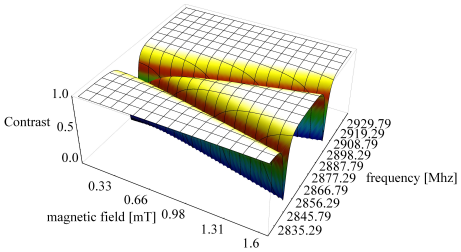

(c) Simulation of the contrast

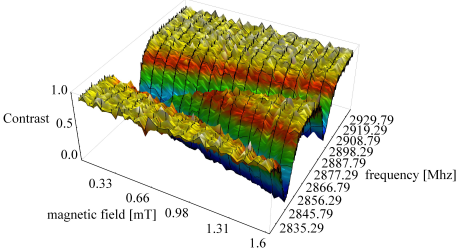

(d) Measurement of the contrast

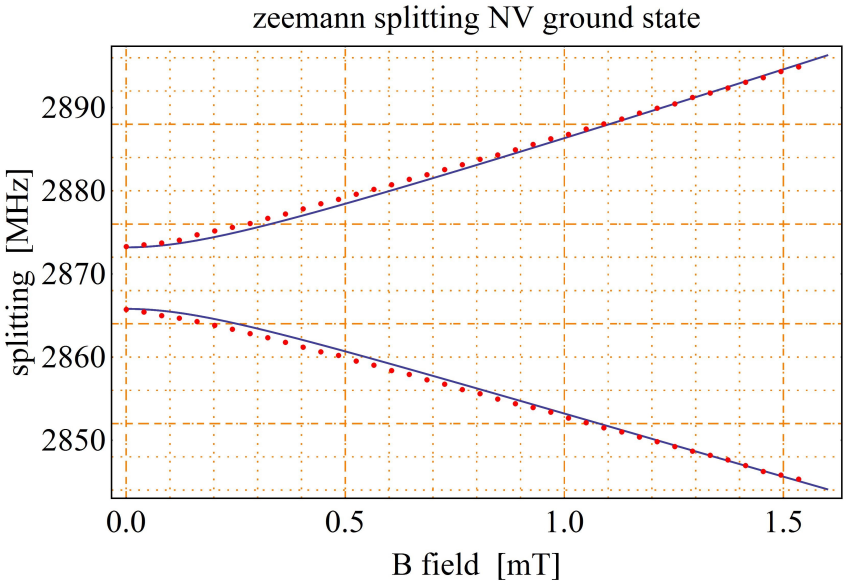

(e) Energy splitting of in dependence of the magnetic field (red points show experimental data and the blue line represents the calculation)

Figure 4.10: Selection of figures which compare energy splitting of the experimental data and the models for $B = (0.5, 0.5, 1)$

4.3.2 Results for a magnetic field direction of (0.5 0.5 1)

Figure 4.11 shows the results of another measurement series. Here the B-field direction was set to $\sim$ (0.5,0.5,1). This means a rotation of the coil over 45°. In this configuration six peaks are visible. Two peaks which are twice as deep as the others because they are degenerate.

The fitting procedure here is a bit more complex because there are more parameters. The fitting function in equation 7 shows that parameter a and g do not depend on the magnetic field. Thus these two parameters were measured at a specific magnetic field and then held fixed for all magnetic fields. In the end there are only three free parameters w_1, w_2 and $w_3 = w_4$. This work is necessary, because if there are too many free parameters in the fit function, the fit doesn't work.

With this fit function the theory and the experiment are compared to each other in figure 4.10 and figure 4.11. It is clear that all measurements match very well with the theory.

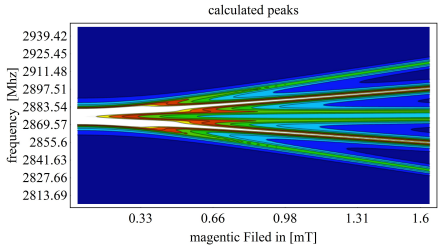

(a) Energy splitting (model)

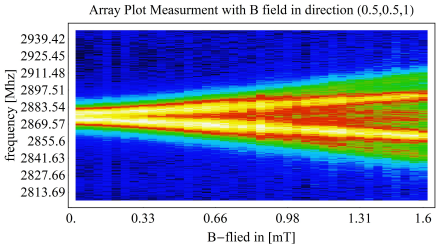

(b) Energy splitting (experiment)

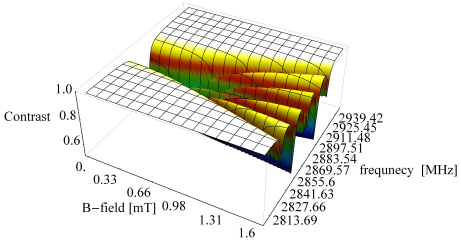

(c) Simulation of the contrast

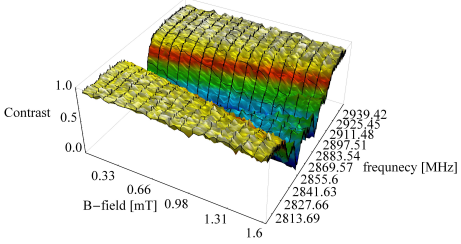

(d) Measurement of the contrast

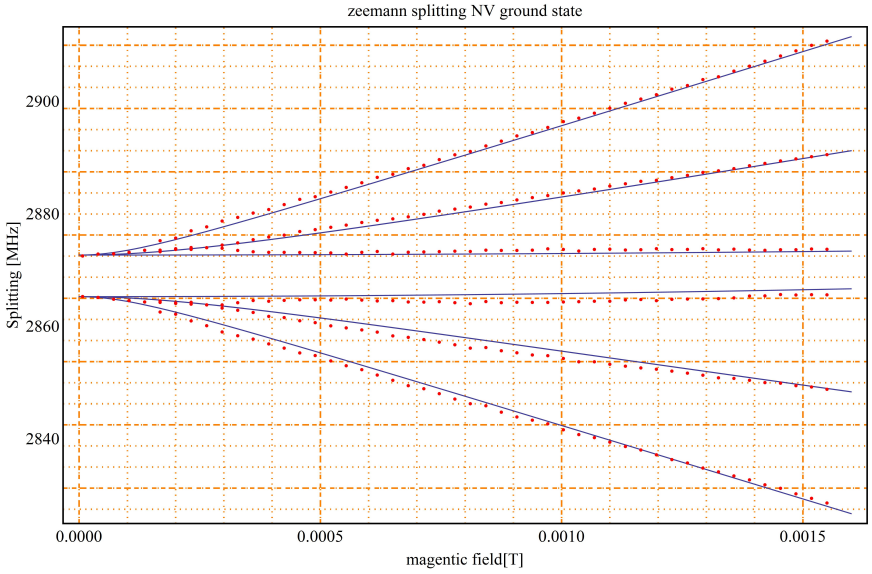

(e) Energy splitting in dependence of the magentic field (red points show experimental data and the blue line represents the calculation)

Figure 4.11: Selection of figures which compare energy splitting of the experimental data and the models for $B \approx (0.5, 0.5, 1)$.

4.4 Estimation of the sensitivity

At this point we want to estimate the theoretical sensitivity of ODMR measurements in the fibre setup. What is the sensitivity of a measurement? If the deviation of the signal is smaller than the noise it is not possible to differentiate between the signal and the noise. The point where the deviation of the signal and the noise have the same value is the interesting point. The fluctuation of the signal at this point is defined as sensitivity. That means that sensitivity is the smallest deviation of the signal which you can see in the measurement.

First the shot noise of the sensor is calculated. Then the maximal gradient of a Lorentzian is calculated. In that way the minimal theoretical sensitivity is calculated.

To calculate the shot noise, first some parameters from the experiment are needed. The basic number is the number of photons which can be counted. That's why the experiment should optimized the experiment in that way. For this reason the detection volume should be maximised. In section 4.2 the experiment is shown. There a single mode fibre with a diameter with $3.4\mu m$ and a $300\mu m$ thick diamond build the sensor volume of $2.7 * 10^{-6} mm^3$. For the optimised setup only one multi mode fibre is used. This fibre has a diameter of $50\mu m$. If we make the assumption that the number of NV centres only depends on the area which is illuminated by the laser a 40 times higher signal is produced. The optimised setup has a detection volume of $9.2 * 10^{-4} mm^3$. The volume rose by a factor for 1000.

In the optimised setup the green laser beam and the red fluorescence are guided through the same multi mode fibre and separated by a dichroic mirror. The signal is so high that it can be measured by an ordinary amplified photo diode (Thorlabs PDA36A-EC). On this photodiode a signal of around 2V (by 70dB amplification) are measured. Through the specification of the photo diode the number of photons are calculated. One assumption in this calculation is that only photons with one wavelength hit the sensor and that only the shot noise limits the signal noise.

$$
\begin{aligned}
&\text{Sensor: PDA36A-EC} \\
&\text{Signal} = 2\text{V} \\
&\text{Gain of 70dB} = 4.75 * 10^5 V/A \\
&\text{dedection efficiency of 700nm} = 0.5 A/W \\
&\text{amplification} = \text{Gain} * \text{dedection efficiency} = 4.7 * 10^5 V/W \\
&\text{Energy of one photon at 635nm } E = \frac{hc}{\omega} = 3.1 * 10^{-19} = 1.95 eV \\
&\text{Signal in Watt} = \frac{Signal}{amplification} = 4.2 * 10^{-6} W \\
&\text{number of photons} = \frac{\text{Signal in Watt}}{\text{Energy of a photon}} = 1.3 * 10^{13} \\
&\text{noise} = \frac{1 * s}{\sqrt{\text{number of photons/s}}} = 2.7 * 10^{-7} \frac{1}{\sqrt{Hz}}
\end{aligned}
\tag{8}
$$

In the next step the sensitivity of the sensor is calculated. The sensitivity is defined as the value where the signal and the noise are equal. The signal is a Lorentzian distribution and is shown in equation 9. In this curve the measurement point is set to the position where the second derivation is zero. This is the best point to measure the magnetic signal because the signal changes most when the field is changing. Here the parameter g is set to 8Mhz (measured in the experiment). In the end we get a sensitivity of $2.2\frac{nT}{\sqrt{Hz}}$.

$$f(x) = \frac{1}{1 + (\frac{x}{g})^2} \tag{9}$$

So how good is that value compared to some other measurement techniques? In figure 4.12 an overview over the best magnetic measurements is given.

In the detail all these techniques are very different. The Squids are very good in the detection volume and in the sensitivity. But their big disadvantage is that they use superconducting devices to measure the field and this works only in a very cold environment. It's also quite problematic to produce the small size of the Squids.

The Hall sensors are very robust but they need electrical components which introduce always electric noise. The vapour cells are very sensitive but for these sensors a volume of gas is needed. This is not so easy to miniaturise.

At last the NV sensors. These defects in diamond have some nice features for the magnetic field measurements. First the NV can be read out just with visible light this is an ideal noise situation. Noise from the environment is no problem because the NV is only affected by a frequency $2.87GHz \pm 200Mhz$. There is no power supply needed for the NV sensor, one noise component less. Another advantage is that the NV centre is very small. It is formed only by two parts: a nitrogen and a vacancy. This is one of the smallest possible structures we can imagine. In addition it is quite stable and robust. The magnetic measurements with NV centres as sensor is not the most sensitive one but they are really unproblematic to use.

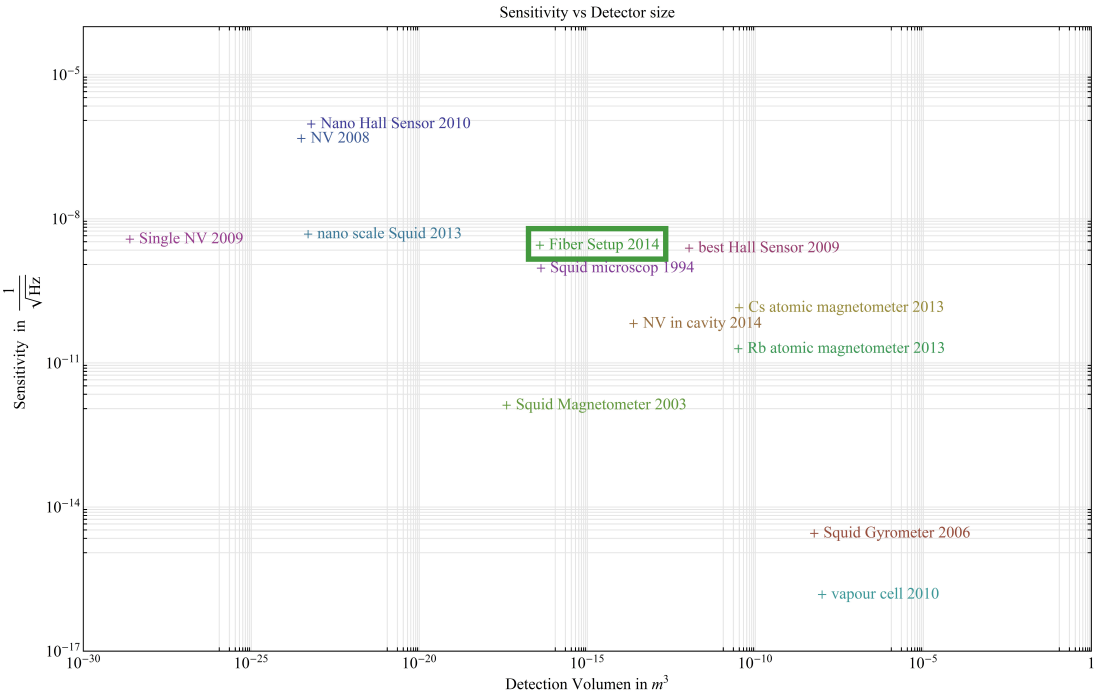

Figure 4.12: Nano Hall Sensor [11], NV [17], Single NV [2], nano scale Squid [24], best Hall Sensor [10], Squid microscope [15], Cs atomic magnetometer [16], Rb atomic magnetometer [23], NV cavity [14], Squid magnetometer [4], vapour cell [21], Squid Gyrometer [9]. The theoretical performance of our setup is framed.

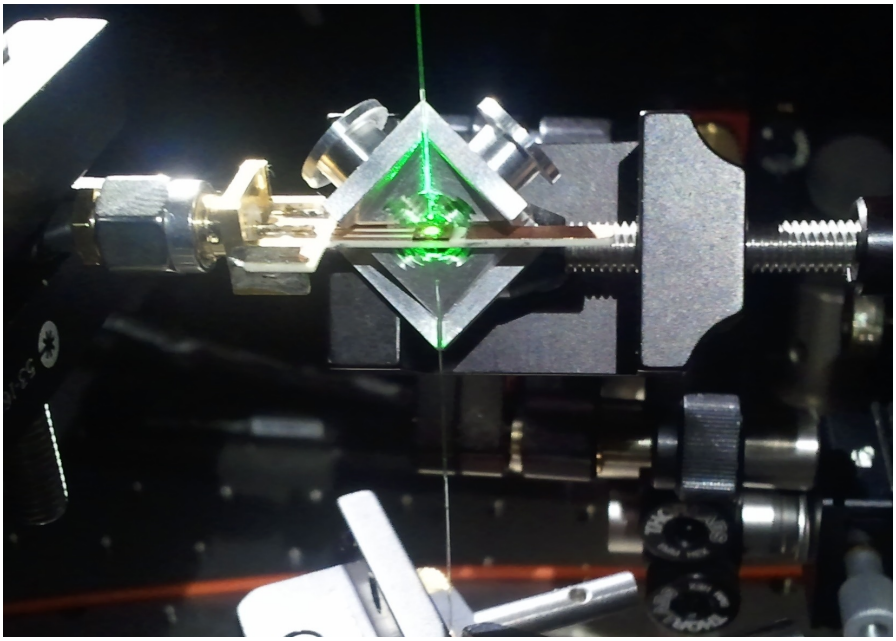

Figure 4.13: The cube in testing position.

4.5 Outlook

In the next step a cube with 6 mini coils is built and surrounds the antenna. In that way it is possible to change the magnetic field in any direction. Each cube part is exactly the same. This cube (see: figure 4.13) is small enough to bring it into a cyrostat and work at liquid nitrogen temperatures. Why is this cube constructed in such a complex way?

Pros

- It is possible to wind the coils before the gluing process of the fibres. This is very important because the fibres and the bonding points break very easily.
- The fibres can be positioned before the cube is closed, which offers the experimenter an essential view.
- The fibre can be fixed before everything is glued.

Cons

- The major problem is to build that cube in the workshop, due to its complex shape.

This new coil structure makes it possible to analyse the ODMR features of the NV centre, measure the strength and a lot of different directions of the field.

5 Rabi oscillations of a two level system

In section 1 NV centres are described as nice quantum systems. So what can be done when laser pulses and microwave pulses are used in combination with NV centres? Rabi oscillations are very interesting. In the first subsection we calculate the Rabi oscillations in a semi classical picture. Then we change to the optical Bloch equations for the full quantum mechanical description and looks on damping effects. Then the Bloch sphere is explained and the Rabi oscillations on a NV are explained [20].

5.1 Rabi oscillations with no damping semi-classical description

A two-level system is the simplest quantum optical system and Rabi oscillations comprise a very general concept. So Rabi oscillations can occur in any system which has two levels with an allowed transition. I usually talk about electron states but Rabi oscillations also occur in spin states of atoms, electrons, neutrons, etc.

The theory starts with two levels $|e\rangle$ and $|g\rangle$, separated by an energy $E_2 - E_1$ (see figure 5.1). The energies of the two levels are given by equation 10. The right wavelength of the transition is given by equation 12. If the energy of an incoming electromagnetic wave ($\hbar\omega$) equals the level spacing one can induce a transition between $|e\rangle$ and $|g\rangle$.

$$\begin{aligned} &|e\rangle \text{ has an energy of } E_2 = \hbar\omega_2 \\ &|g\rangle \text{ has an energy of } E_1 = \hbar\omega_1 \end{aligned} \tag{10}$$

The Hamiltonian $\hat{H}$ can be written as the sum of the homogeneous Hamiltonian $\hat{H}_0$ and the influence of the incoming photons $\hat{d}\vec{E}(t)$, the dipole operator times the field.

$$\hat{H} = \hat{H}_0 + \vec{d}\vec{E}(t) \tag{11}$$

$$\omega_{21} = \omega_2 - \omega_1 \tag{12}$$

$$\begin{aligned} \hat{H}_0 &= \hbar\omega_2 \left|2\right\rangle \left\langle 2\right| + \hbar\omega_1 \left|1\right\rangle \left\langle 1\right| \\ \vec{E} &= \vec{\epsilon} E_0 cos(\omega t) \end{aligned} \tag{13}$$

We are interested in the time evolution of this situation and thus want to solve equation 14. To solve this differential equation, we make the ansatz shown in equation 15. Together with the definition of d_{12} (see equation 16) we can rewrite our equation to 17 and define the Rabi frequency as Ω_0 (see equation 18).

$$i\hbar \frac{\partial \left|\phi(t)\right\rangle}{\partial t} = \hat{H} \left|\phi(t)\right\rangle \tag{14}$$

$$\text{Ansatz: } \left|\phi(t)\right\rangle = C_1(t) e^{-i\omega_1 t} \left|1\right\rangle + C_2(t) e^{i\omega_2 t} \left|2\right\rangle \tag{15}$$

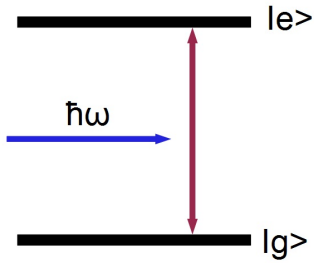

Figure 5.1: Here the energy levels of a two level system are shown. $\hbar\omega$ is the energy of an incoming electromagnetic wave.

$$d_{12} = \langle 1|\, \hat{d\vec{\epsilon}}|2\rangle = e\,\langle 1|\, \vec{r\epsilon}|2\rangle = d_{12}^* = d \tag{16}$$

$$\begin{aligned} i\hbar\dot{C}_1(t) &= -d_{12}E_0 e^{-i\omega_{21}t} cos(\omega t) C_2(t) \\ i\hbar\dot{C}_2(t) &= -d_{21}E_0 e^{i\omega_{21}t} cos(\omega t) C_1(t) \end{aligned} \tag{17}$$

$$\Omega_0 = \frac{dE_0}{\hbar} \tag{18}$$

At this point the equation is going to be simplified and therefore we are looking for terms which can be neglected. We rewrite $\cos(\omega t)$ as shown in equation 19 and use it together with the Rabi frequency to simplify equation 17 to equation 20. Now we can identify two terms of the form $\omega_{12} + \omega$ as fast oscillation terms, which can be neglected if $|\omega_{12} - \omega| \ll \omega_{12}$. This simplification is called rotating wave approximation.

$$cos(\omega t) = \frac{(e^{i\omega t} + e^{-i\omega t})}{2} \tag{19}$$

$$\begin{aligned} \dot{C}_1(t) &= \frac{i\Omega_0}{2}(e^{-i(\omega_{21}-\omega)t} + \underbrace{e^{-i(\omega_{21}+\omega)t}}_{neglected})C_2(t) \\ \dot{C}_2(t) &= \frac{i\Omega_0}{2}(\underbrace{e^{+i(\omega_{21}+\omega)t}}_{neglected} + e^{+i(\omega_{21}-\omega)t})C_1(t) \end{aligned} \tag{20}$$

In equation 21 δ is defined. δ is the difference between resonant wavelength ω_{12} and the wavelength of the incoming wave, ω:

$$\delta = \omega - \omega_{21} \tag{21}$$

$$\begin{aligned} \dot{C}_1(t) &= \frac{i\Omega_0}{2} e^{i\delta t} C_2(t) \\ \dot{C}_2(t) &= \frac{i\Omega_0}{2} e^{-i\delta t} C_1(t) \end{aligned} \tag{22}$$

$$\begin{aligned} \widetilde{C}_1 &= C_1(t)e^{-i\frac{\delta}{2}t} \\ \widetilde{C}_2 &= C_2(t)e^{i\frac{\delta}{2}t} \end{aligned} \tag{23}$$

$$\frac{d}{dt}\begin{pmatrix}\widetilde{C}_1(t)\\ \widetilde{C}_2(t)\end{pmatrix} = \frac{i}{2}\begin{pmatrix}-\delta & \Omega_0\\ \Omega & \delta\end{pmatrix}\begin{pmatrix}\widetilde{C}_1(t)\\ \widetilde{C}_2(t)\end{pmatrix} \tag{24}$$

5.1.1 Rabi oscillations with no detuning

In this subsection the detuning is set to zero ($\delta = 0$), this is the resonant case. That means there is no difference between ω_{12} and ω. So the energy of the incoming wave and the energy difference of the levels are the same.

To solve this system of differential equations some boundary conditions are needed: At time t=0 all electrons are supposed to be in the ground state and none in the excited state.

$$\begin{aligned} &\text{simple case: } \delta = 0 \\ &C_1(0) = 1 \text{ and } C_2(0) = 0 \\ &\dot{\widetilde{C}}_1(t) = i\frac{\Omega_0}{2}C_2(t) \\ &\ddot{\widetilde{C}}_1(t) = i\frac{\Omega_0}{2}\dot{C}_2(t) = -i\frac{\Omega_0^2}{4}\widetilde{C}_1(t) \end{aligned} \tag{25}$$

$$\begin{aligned} \widetilde{C}_1 &= \cos(\frac{\Omega_0 t}{2}) \\ \widetilde{C}_2 &= i\sin(\frac{\Omega_0 t}{2}) \end{aligned} \tag{26}$$

$$P_{12}(t) = \left|\widetilde{C}_2(t)\right|^2 = sin^2(\frac{\Omega_0 t}{2}) = \frac{1}{2}(1 - cos(\Omega_0 t)) \tag{27}$$

In equation 27 the first result is shown. P_{12} gives the possibility to find an electron in the excited state. A very important remark is that these equations only work well at the start of the oscillation because in this case damping effect can be neglect. However with this restriction we can think about some special cases. They are shown in equation block 28.

π pulse: $\tau = \dfrac{\pi}{\Omega_0}$
$P_{12}(\tau) = 1$
$\Rightarrow$ population inverted

$\dfrac{\pi}{2}$pulse:
$\Rightarrow \widetilde{C}_1(\tau) = \dfrac{1}{\sqrt{2}}$ and $\widetilde{C}_2(\tau) = \dfrac{i}{\sqrt{2}}$
$\Rightarrow |\phi\rangle = \dfrac{1}{\sqrt{2}}(|1\rangle + i\,|2\rangle)$
$\Rightarrow$ system in superposition between ground and excited state (28)

2π pulse: $\tau = \dfrac{2\pi}{\Omega_0}$
$\widetilde{C}_1(\tau) = -1$ and $\widetilde{C}_2(\tau) = 0$
$|\phi(\tau)\rangle = -\,|\phi(0)\rangle$
global phase of state changed sign

4π pulse:
$2 * 2\pi$ back in the initial state (SU(2)-symmetry)

The first case is the π pulse. That means that the time of the incoming photon pulse has a value of $\frac{\pi}{\Omega_0}$. All pulses are in the unit of $\frac{1}{\Omega_0}$, so if somebody talks about π pulses that makes that sense if Ω_0 is known. After applying a π pulse the whole population is inverted. All electrons of the excited state are in the ground state and vice versa.

Another interesting pulse is the $\frac{\pi}{2}$ pulse. This pulse brings the system in a superposition of the ground and the excited state. That means that the possibility to find the electron in the excited state is 50%.

With a 2π pulse the sign of the global phase is changed and after a 4π pulse the system is back to the initial state. These are the properties of the SU(2)-symmetry of a spin system.

5.1.2 Rabi oscillations with detuning

In this subsection we look at what happens if there is detuning. In equation 29 the solution of this case is noted. The detuning brings two additional effects:

- The oscillation amplitude gets smaller. That means that the possibility to find the electron in the excited state is not one anymore after a π pulse.

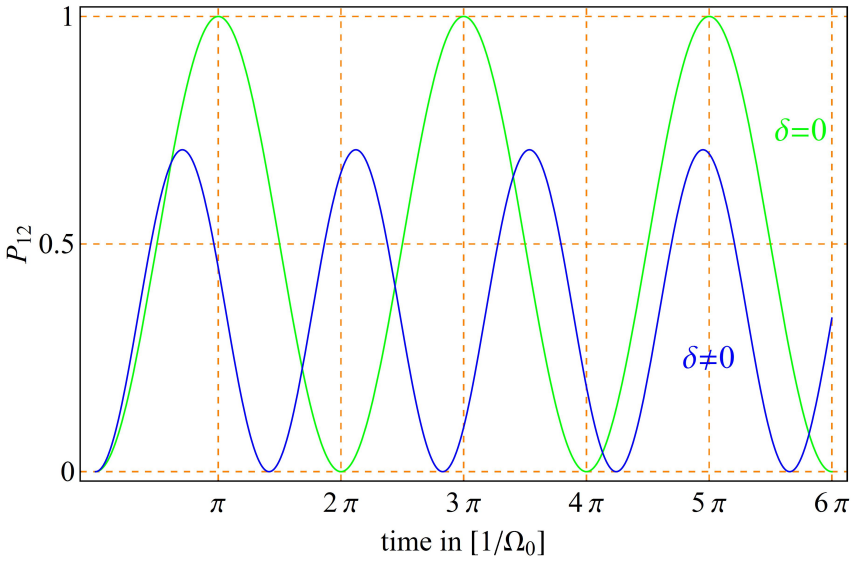

Figure 5.2: Here the possibility P_{12} with $\delta = 0$ (equation 27) and P_{12} with $\delta \neq 0$ (equation 29) are plotted.

- The frequency gets higher.

$$\begin{aligned} &\delta \neq 0 \\ &\text{solution for } \widetilde{C}_1(0) = 1 \text{ and } \widetilde{C}_2(0) = 0 \\ &P_{12}(t) = \left|\widetilde{C}_2(t)\right|^2 = \frac{\Omega_0^2}{2\Omega}(1 - cos(\Omega t)) \\ &\text{with } \Omega = \sqrt{\Omega_0^2 + \delta^2} \text{ and } \delta = \omega - \omega_{12} \end{aligned} \tag{29}$$

5.2 Rabi oscillations with damping and detuning described as density matrix

The previous calculations only describe the start of the oscillations very well. But what will happen afterwards? In a real measurement damping will always occur. By adding spontaneous emission in the equation one can account for this phenomenon. For analysing this process the full quantum mechanical description is used in this case by the density matrix in the interaction picture.

$$
\begin{aligned}
&\hat{\rho} = |\phi\rangle \langle\phi| \\
&\text{with } |\phi(t)\rangle = C_1(t)e^{-i\omega_1 t}|1\rangle + C_2(t)e^{i\omega_2 t}|2\rangle \\
&\hat{\rho} = \begin{pmatrix} \rho_{11} & \rho_{12}* \\ \rho_{21}* & \rho_{22} \end{pmatrix} = \begin{pmatrix} C_1C_1^* & C_1C_2^* \\ C_2C_1^* & C_2C_2^* \end{pmatrix}
\end{aligned} \tag{30}
$$

So $\rho_{11} = |C_1(t)|^2$ describe the population of the state $|1\rangle$ and $\rho_{22} = |C_2(t)|^2$ is the population of state $|2\rangle$. The off diagonal elements describe the coherence between state $|1\rangle$ and $|2\rangle$. If these elements disappear there is no phase relationship between both states. Let's have a look at the time dynamics of the density elements.

$$
\begin{aligned}
&\dot{\rho}_{11} = \dot{C_1}C_1^* + C_1\dot{C_1}^* = \frac{i\Omega_0}{2}(e^{i\delta t}\rho_{12}^* - e^{-i\delta t}\rho_{12}) \\
&\text{see equation 22 for the definition of C and } \dot{C}
\end{aligned} \tag{31}
$$

That's a good point to make this equation a little bit simpler. When we substitute $e^{-i\delta t}\rho_{12}$ with $\widetilde{\rho}_{12}$ we get the following expressions:

$$
\begin{aligned}
\widetilde{\rho}_{12} &= e^{-i\delta t}\rho_{12} \\
\dot{\rho}_{11} &= \frac{i\Omega_0}{2}(\widetilde{\rho}_{12}^* - \widetilde{\rho}_{12}) \\
\dot{\rho}_{22} &= i\frac{\Omega_0}{2}(\widetilde{\rho}_{12} - \widetilde{\rho}_{12}^*) \\
\dot{\widetilde{\rho}}_{12} &= -i\delta\widetilde{\rho}_{12} + i\frac{\Omega_0}{2}(\rho_{22} - \rho_{11})
\end{aligned} \tag{32}
$$

In all equation before there was no damping. At this point the damping rate is added to the equations. The damping rate is phenomenological. It describes the spontaneous emission. Equation 33 is called the optical Bloch equation and describes the atom-light interaction.

$$
\begin{aligned}
\dot{\rho_{11}} &= \gamma\rho_{22} + i\frac{\Omega_0}{2}(\widetilde{\rho}_{12}^* - \widetilde{\rho}_{12}) \\
\dot{\rho_{22}} &= -\gamma\rho_{22} + i\frac{\Omega_0}{2}(\widetilde{\rho}_{12} - \widetilde{\rho}_{12}^*) \\
\dot{\widetilde{\rho}}_{12} &= -(\frac{\gamma}{2} + i\delta)\widetilde{\rho}_{12} + i\frac{\Omega_0}{2}(\rho_{22} - \rho_{11})
\end{aligned} \tag{33}
$$

The factor γ describes the damping rate.

Rabi oscillations should be damped oscillations. For the case that $t << \frac{1}{\gamma}$ and $\Omega_0 > \gamma$ the spontaneous emission can be neglected and Rabi oscillations can be observed. For the case $t >> \frac{1}{\gamma}$ the stationary solution is found.

5.3 Bloch vector and Bloch sphere

The Bloch vector and the Bloch sphere are nice representations of the optical Bloch equations. With them a lot of complex problems can be solved in a very easy way. It is easy to control the calculation with a plot. The Bloch vector $\vec{u}$ is defined in equation 34.

$$\begin{aligned}
&\vec{u} = (u, v, w)\\
&u = \widetilde{\rho}_{12} + \widetilde{\rho}_{12}^{*} = 2\ Re(\widetilde{\rho}_{12})\\
&v = i(\widetilde{\rho}_{12} - \widetilde{\rho}_{12}^{*}) = 2\ Im(\widetilde{\rho}_{12}))\\
&w = \rho_{22} - \rho_{11}\\
&u\text{: Dispersive part of the Bloch vector}\\
&v\text{: Absorptive part of the Bloch vector}\\
&w\text{: Population inversion}
\end{aligned} \tag{34}$$

From a physical point of view, everything is in the ground state if the population inversion w=-1. So the probability to find the electrons in the ground states equals one. For w=1 all electrons are in the excited state. The physical meaning of w and v is a little bit more complexer. I will show that an following example: expectancy value values of the dipole operator:

density matrix in interaction picture

$$\hat{\rho} = \begin{pmatrix} \rho_{11} & \rho_{12} * e^{-i\omega t} \\ \rho_{21} * e^{i\omega t} & \rho_{22} \end{pmatrix} = \begin{pmatrix} C_1 C_1^{*} & C_1 C_2^{*} e^{i\omega t} \\ C_2 C_1^{*} e^{-i\omega t} & C_2 C_2^{*} \end{pmatrix} \tag{35}$$

$$\begin{aligned}
&< \hat{d} >= trace(\hat{\widetilde{\rho}}\hat{d}) = trace\left(\begin{pmatrix} \tilde{\rho_{11}} & \tilde{\rho_{12}} e^{-i\omega t} \\ \tilde{\rho_{21}} e^{i\omega t} & \tilde{\rho_{22}} \end{pmatrix} \begin{pmatrix} 0 & \vec{d}_{12} \\ \vec{d}_{12} & 0 \end{pmatrix}\right)\\
&\text{with: } d_{12} = d_{21} \text{because } d_{12} \text{ is real}\\
&< \hat{d} >= d_{21}(\tilde{\rho_{21}} e^{i\omega t} + \tilde{\rho_{12}}^{*} e^{-i\omega t}) = \vec{d}_{12}(u\ cos(\omega t) - v\ sin(\omega t))\\
&\text{with: } e^{\pm i\omega t} = cos(\omega t) \pm i sin(\omega t)
\end{aligned} \tag{36}$$

If the field is given by $\vec{E}(t) = \vec{\epsilon} E_0 cos(\omega t)$ it is possible to say that:

- u stands for the coupling with the dipoles which oscillate in phase with the field.
- v stands for the coupling with the dipoles which oscillate 90°C out of phase with the field.

With the definition given by equation 34, equation 33 can be rewritten in the following form:

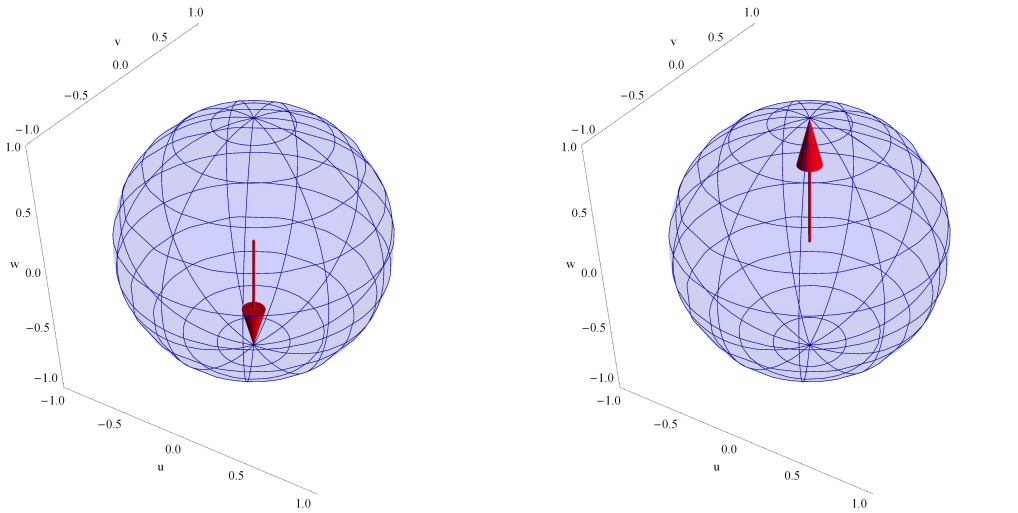

(a) Bloch vector for w=-1 means $\vec{u} = (0, 0, 1)$ and $|\phi\rangle = |1\rangle$.

(b) Bloch vector for w=1 means $\vec{u} = (0, 0, -1)$ and $|\phi\rangle = |2\rangle$.

Figure 5.3: The ground and excited state of the Bloch vectors

$$\frac{d}{dt}\begin{pmatrix} u \\ v \\ w \end{pmatrix} = -\begin{pmatrix} \Omega_0 \\ 0 \\ \delta \end{pmatrix} \times \begin{pmatrix} u \\ v \\ w \end{pmatrix} - \gamma \begin{pmatrix} \frac{u}{2} \\ \frac{v}{2} \\ w+1 \end{pmatrix} \tag{37}$$

For a better understanding of this differential equation γ is set to zero. That means there is no damping. Then the formula 37 looks like the angular momentum operator in the classical mechanics:

$$\frac{d}{dt}\vec{u} = -\vec{\Omega} \times \vec{u} \text{ with: } \vec{\Omega} = (\Omega_0, 0, \delta) \text{ and } \vec{u} = (u, v, w) \tag{38}$$

Analogous to the equation of motion of the spinning top, $-\Omega$ is named the angular velocity of the Bloch vector. It is possible to show that in the case without damping the Bloch vector always lies on the Bloch sphere. So the condition $u^2 + v^2 + w^2 = 1$ is fulfilled. For the case of damping the vector $\vec{u}$ decreases with time. So the condition $u^2 + v^2 + w^2 \leq 1$ is fulfilled in any case. In equation 28 a lot of cases can be calculated directly. All of these results must be also true for the Bloch vector equation because they are representations of the same problem. However the Bloch vectors have the big advantage that they can be plotted easily.

In figure 5.3 the two simplest cases of the Bloch vectors are plotted. Next it is shown what happens when a $\frac{\pi}{2}$ pulse is applied in the case of ρ equals to zero. So the Bloch vector goes from the bottom of the sphere to the equator and begins to rotate with a frequency of ω in phase with the E-field. Mathematically the state $|1\rangle$ goes to $\frac{1}{\sqrt{2}}(|1\rangle + i\,|2\rangle)$ which means that $\vec{u} = (0, 0, -1)$ transform to $\vec{u} = (0, -1, 0)$.

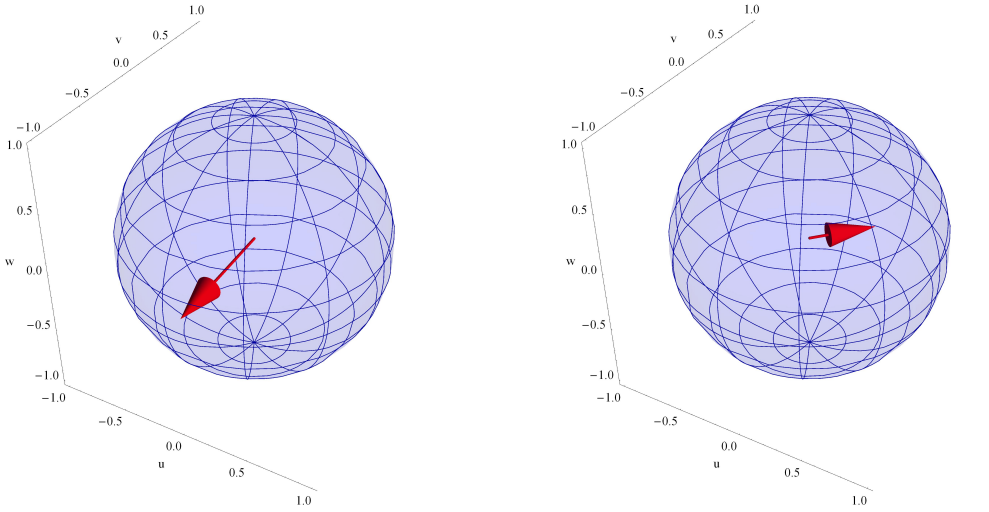

(a) Bloch vector with initial vector $\vec{u}$=(0,0,-1) after a $\frac{\Pi}{2}$ pulse

(b) Bloch vector $\vec{u}$ including damping

Figure 5.4: Bloch vector for a mixed state with damping

5.3.1 Damping in the Bloch vector

However in the experiment neither the damping rate nor ρ will equal zero. So what happen in that case? Equation 37 tells us that if γ is not zero there are two different sources of damping. The first is the term $-\gamma(w+1)$ this term is produced by the spontaneous emission. If we set the initial state to (0,0,1) (excited state) the term $-\gamma(w+1)$ transfers everything to (0,0,-1) (ground state). This term is only zero for the case that the system is in the ground state (w=-1).

The other source of damping is described by $-\gamma(\frac{u}{2}, \frac{v}{2})$. This term damps the vector in the u,v plane. This fundamental damping results from the uncertainty principle and in the end it is observed as a shift of the phase.

There is no possibility to avoid this damping in the experiment. The finite lifetime of the excited state is the reason for these two damping effects. But here we want to work with NV centres, they are defect centres in a solid body. That means that there are more existing damping terms. Therefore an additional γ^* has to be built in:

$$\frac{d}{dt}\begin{pmatrix} u \\ v \\ w \end{pmatrix} = -\begin{pmatrix} \Omega_0 \\ 0 \\ \delta \end{pmatrix} \times \begin{pmatrix} u \\ v \\ w \end{pmatrix} - \gamma \begin{pmatrix} 0 \\ 0 \\ w+1 \end{pmatrix} - \gamma^* \begin{pmatrix} u \\ v \\ 0 \end{pmatrix} \tag{39}$$

The new damping rate γ^* includes a lot of effects. But in general the damping rates can be assigned to two groups. The random part is noise from the environment(magnetic fields, radio waves, the other spins from the carbon,...). The other source is more systematic: angle variations of different families of NV centres due to stress in the crystal and other spins in the diamond. This systematic parts could be fixed with spin echo

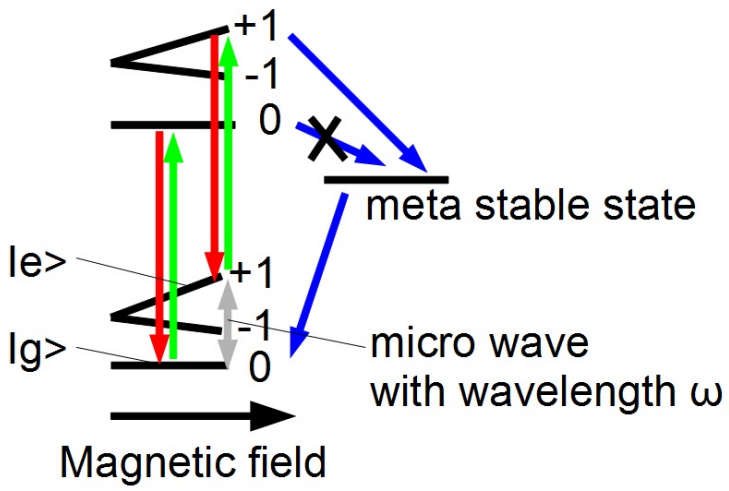

Figure 5.5: In this figure all necessary levels for the Rabi oscillation are shown. The green arrows represent the green laser light, the red are the fluorescence, the blue ones are non radiative transitions and the grey one represent the microwave. The blue arrow with the black cross is a not allowed transition. The Rabi oscillations between the $m_s = 0$ and the $m_s = 1$ state of the ground state will be driven. The excited state and the metastable levels are only needed for the read out process.

methods. The fundamental part is discussed in the last part. So it is possible to say that the damping shortens the Bloch vector.

5.3.2 The Bloch vector including detuning

What happens if $\rho \neq 0$? In figure 5.2 the effect for $\rho \neq 0$ is shown for the case without damping. The same happens with the Bloch vector: the vector rotates with the frequency ω and a shift of ρ. For example in the case of a $\frac{\pi}{2}$ pulse with $\rho \neq 0$ there is a phase shift of $\delta\phi = -\rho t$ which occurs between the oscillation of the dipoles and the oscillation of the light field.

5.4 Rabi oscillations of the NVs centres

In the last section the Rabi oscillations for NV centres were calculated. The question at this point is which levels should be used for the Rabi oscillations and how they can be measured. In figure 5.5 all involved levels are shown.

For the two level system the $m_s = 0$ and the $m_s = +1$ of the ground level are used. The electromagnetic wave is a pulsed microwave source and the readout of the spin state works via the metastable state. How does that work?

The first step is to create a π pulse with the microwave. When the pulse has the right length all electrons are in the spin +1 state. Then a short green pulse pumps the electrons in the m_s =+1 state of the excited state. From there there is a probability

of around 50% that the electron falls to the metastable level. So this electron is held for a while. The short green pulse produces a fluoresce signal. The intensity of this signal depends directly on the number of electrons in the $m_s = 0$ state. That means that if all electrons are in the $m_s = 0$ state there are no losses to the metastable state and the maximum signal is measured. If all electrons are in the $m_s = 1$ state the signal decreases. So for a variation of the pulse length of the microwave signal, the fluorescence signal should behave like a sine wave.

Then a second long green pulse is sent. This long green pulse induces a big increase of the damping term so that in the end the NV centre is in the $m_s = 0$ state. At this time an good initial state is reached and the whole process can be repeated.

6 Outlook

What are the next steps in this experiments?

At first it should be fine to make the measure process for the ODMR faster. The limiting devise for this is the frequency generator. This generator if very precise but he need more then 10ms for changing his frequency. So in one second only 100 points are measured. We want to replace them with an voltage controlled oscillator (VCO). This VCO is not so precise put he is very fast. With the VCO it should be possible to built an real time NV magnetometer. The aim of this future application is to make this measurement as fast as possible. The physical restriction is the lifetime of the metastable state. It should be possible to measure with a repetition of 1kHz without any problems. We think that we can build a tabletop device which measures the strength and the direction of a magnetic field outside of a lab environment.

An other future project is to bring ODMR experiments inside an cold environment (4K liquid Helium). For this experiment the cube (see:4.13) are designed. The low temperature reduce the phonon side bands and has an effect on the frequency of the level splitting. In this experiment it is also possible to set the field direction in any direction we want.

Than we want to build a microwave switch into the setup to find Rabi oscillations in the experiment. In that way we want look at the different damping times of the NV. There are three damping times in the Rabi oscillations which we want to separate with different methods. At first the T_1 this time is induced as spontaneous emission of the excited state. This time is in all different measurements the same. There are also two other damping times T_2 and T_2^* these terms produce an phase shift in NV spin system. The different between T_2 and T_2^* is that T_2 include non-reversible processes and T_2^* include all reversible processes. To different theses two times we need to replace the HF-switch by a Q-switch. This Q-switch make it possible to work with x- and y-pulses for highly effective spin echo methods. How does that work? For one spin we can make the following procedure. We begin in the ground state and start this pulse train $\left(\frac{\pi}{2}\right)_x$ pulse, wait, $\left(\frac{\pi}{2}\right)_x$ pulse. Then we are in the excited sate. For many spins this is not so easy because there deviation in the axis of the NV centres. So the spins don't overlay after the second $\frac{\pi}{2}$ pulse. To prevent this we could send another pulse train like $\left(\frac{\pi}{2}\right)_x$

pulse, wait, $(\pi)_y$ pulse, wait, $\left(\frac{\pi}{2}\right)_x$ pulse. In this case the reverse able effects of the damping are subtracted out and we can different between T_2 and T_2^*.

Why we are interested in these damping effects? For the different applications of NV centres it is important to characterise their property to optimise the production conditions. For quantum information systems it is very interesting to know how long the spin stage storage by the system can be.

So we hope that we can build a faster and smaller ODMR device and have a look at Rabi oscillations and pulse sequences to measure the different damping rates of NV centres in diamonds.

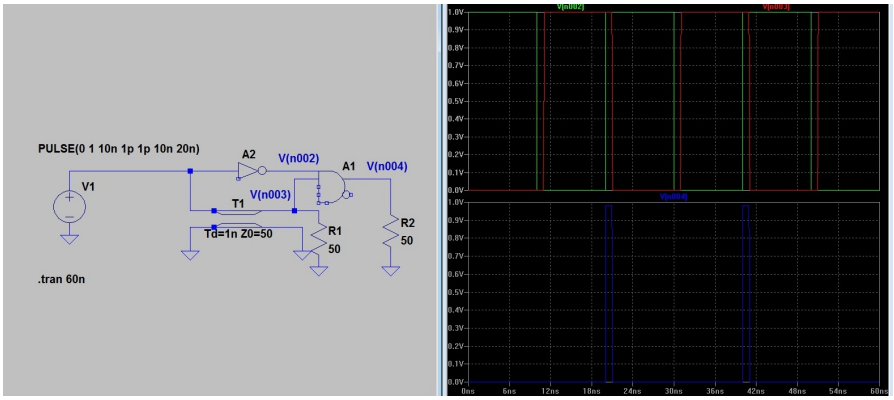

Figure A.1: concept of ns pulse production

A How to build your own pulsed diode laser

The problem with a real fast driver is not the driver itself but the electric logic which should drive it. A normal logic signal like a TTL (transistor transistor logic) has a rising and falling time of about 50ns. So it is very important to build a fast logic. The aim of this driver was a switching time of about 1-2ns. That means that the rising and the falling time of the logic must be in the range of 1 ns or less. There are some logic families which are fast enough. For this driver an ECL (Emitter couple logic) is used. In an ordinary slow logic the transistors are open or closed. In the ECL the transistors are in a dynamic regime, they are half open and can be switched very fast in a range down to 100ps. In this case ECL is build as a differential logic. So the signal does not depend on the absolute value. The difference between the two signal wire is the criterion of zero and one. This needs a special termination of 50ohm but with one ground and two signals there are more possibilities in which way the termination can be build. [18]
The first task was to produce a ns pulse by means of latches. Usually they induce problems by the synchronization of signal propagation delays, but in this case they are very good. The trigger signal from the outside goes through a TTL to ECL converter. Then the line is split into two. Each of these lines run throw a time delay chip. With a minimal delay of 1ns and a maximal delay of 10ns. One of these lines is inverted. At the end these two lines are linked with an AND gate. This produces the nice ns latch. (see figure A.1)

For this thesis three of these laser drivers were built. Here the schematic of the circuit which works best is shown.

The next step is the laser diver. Before the lasers are integrated in the setup the dynamics of the laser diodes must be checked. So the rising and the falling time must be measured. For this an evaluation board is the best idea [13] . For this test the evaluation board of a special driver chip (IC-Hause IC-HG) is used. This chip is also built into the driver circuit. It is important to know how fast the diodes are.

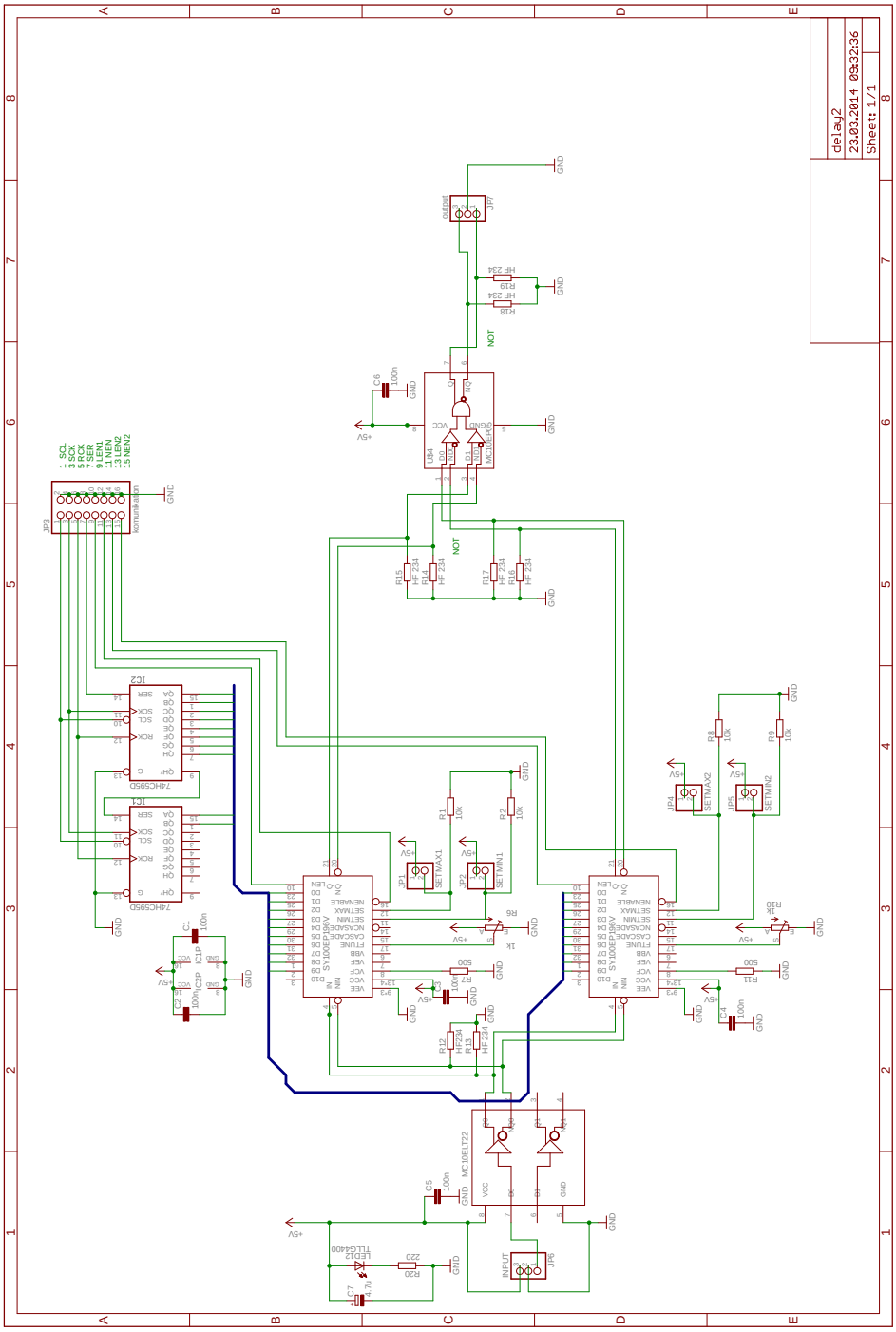

Figure A.2: Schematics of delay circuit

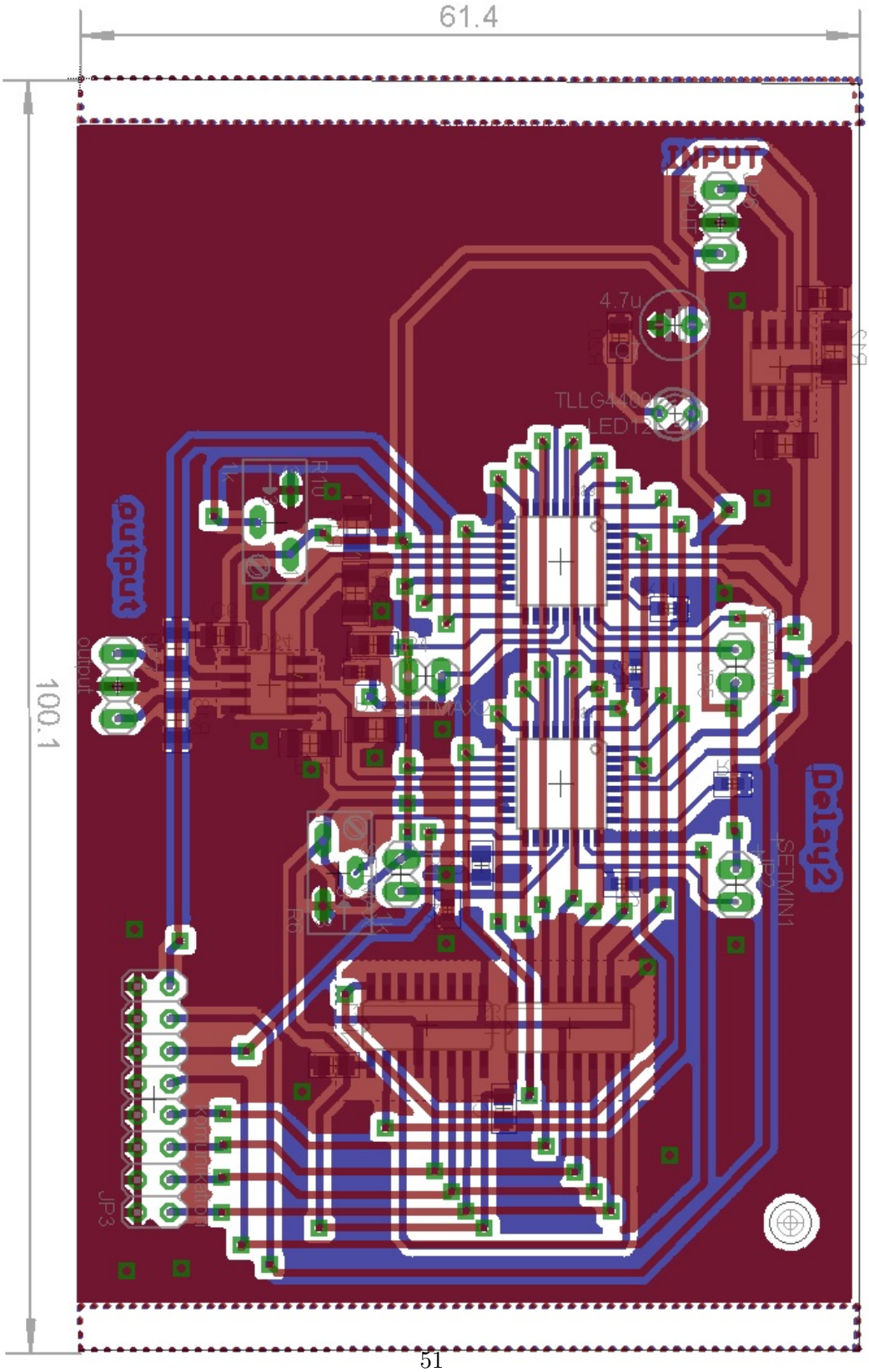

Figure A.3: Board of the delay circuit

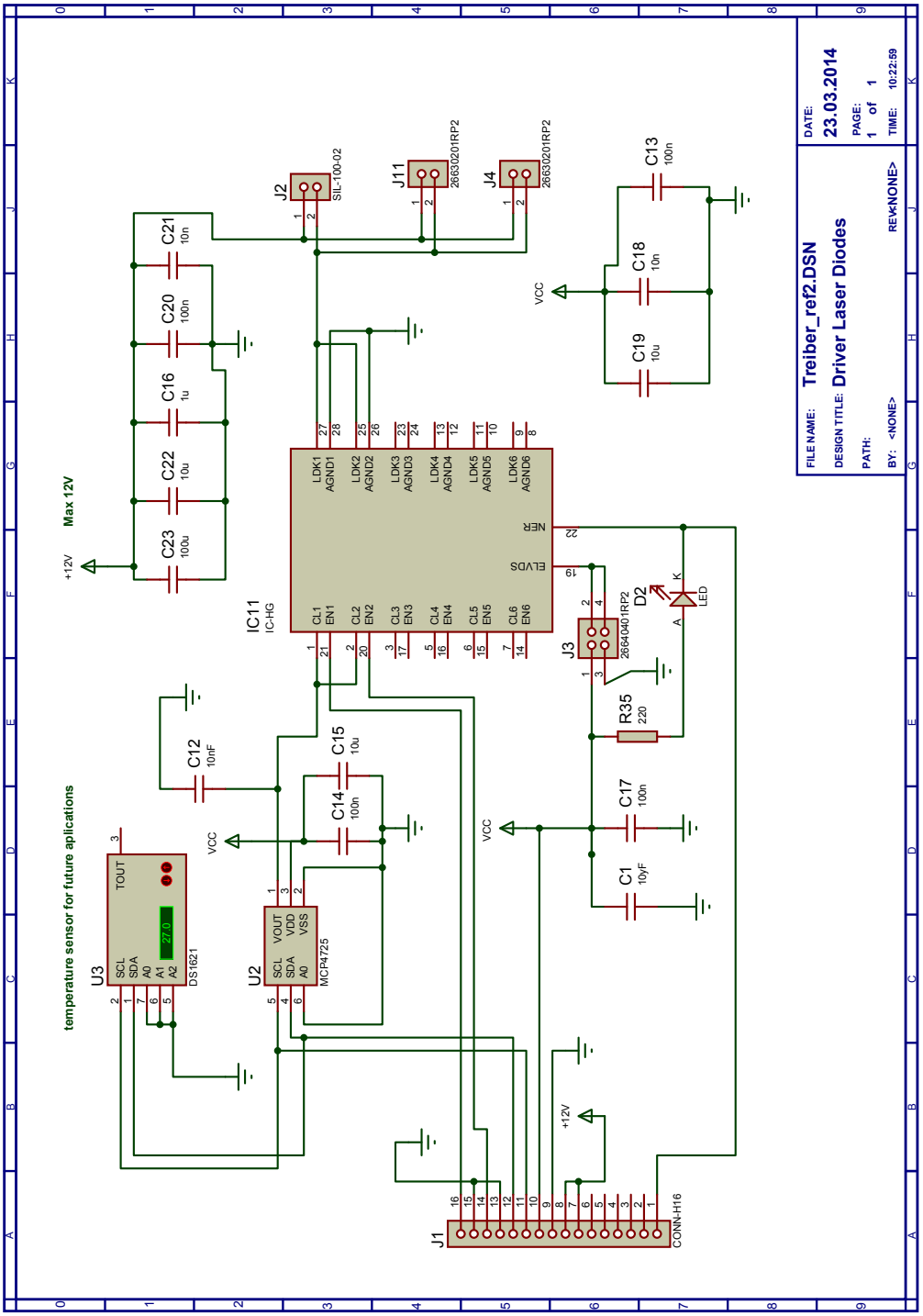

Figure A.4: Schematics of the driver circuit

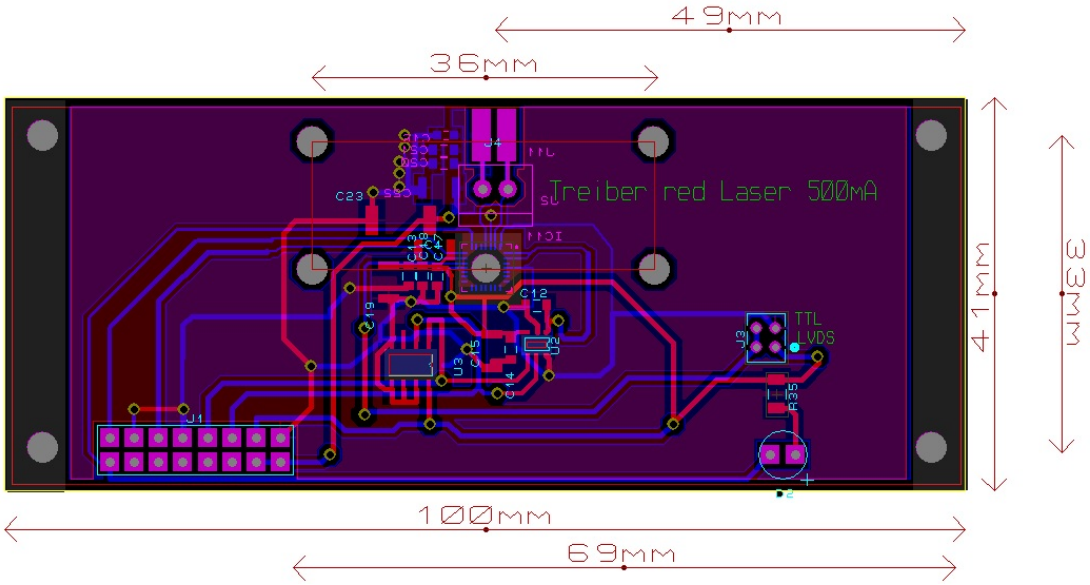

Figure A.5: Board of delay circuit

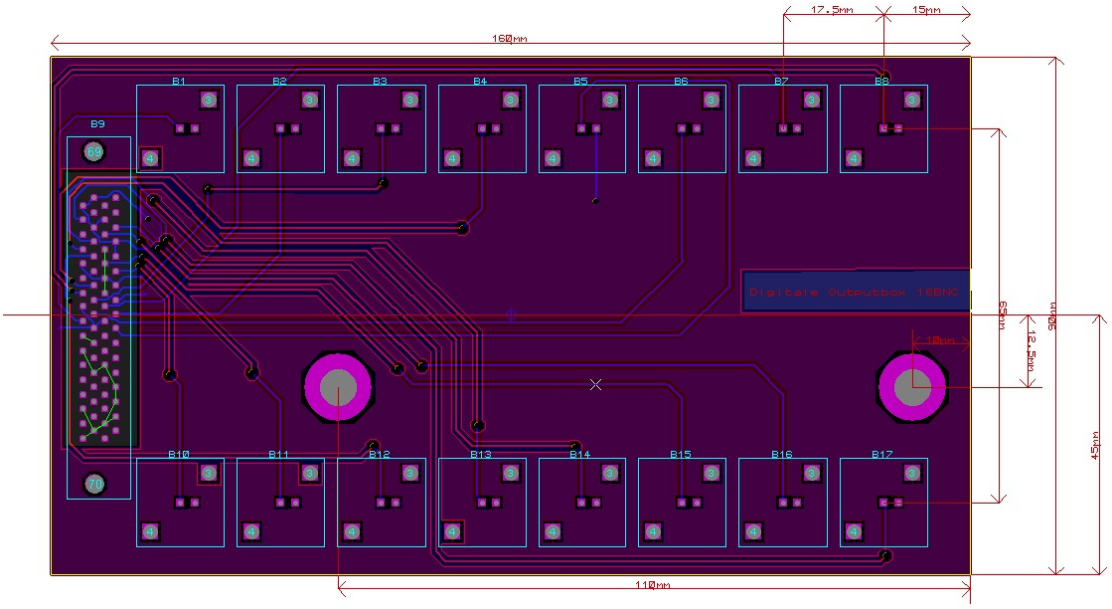

Figure B.1: Layout of the Output-box

B Output-box for a National Instruments Card

In this section it is shown how to build a digital output box for a labview card. They were needed because only two normal digital outputs on the original output box (National Instruments 2090A) were build in. The biggest problem was the socket because the numbering was arranged in a non natural way. Be very careful if you should plan to build a circuit board with a socket with 68 pins!

Anzahl	Bezeichnung	Farnellbestellnumer
16	BNC-stehend	1712351
1	86 HARTING buchse 90	1142818
2	86 HARTING stecker Flachband	1096975
1	box europlatine	4744810

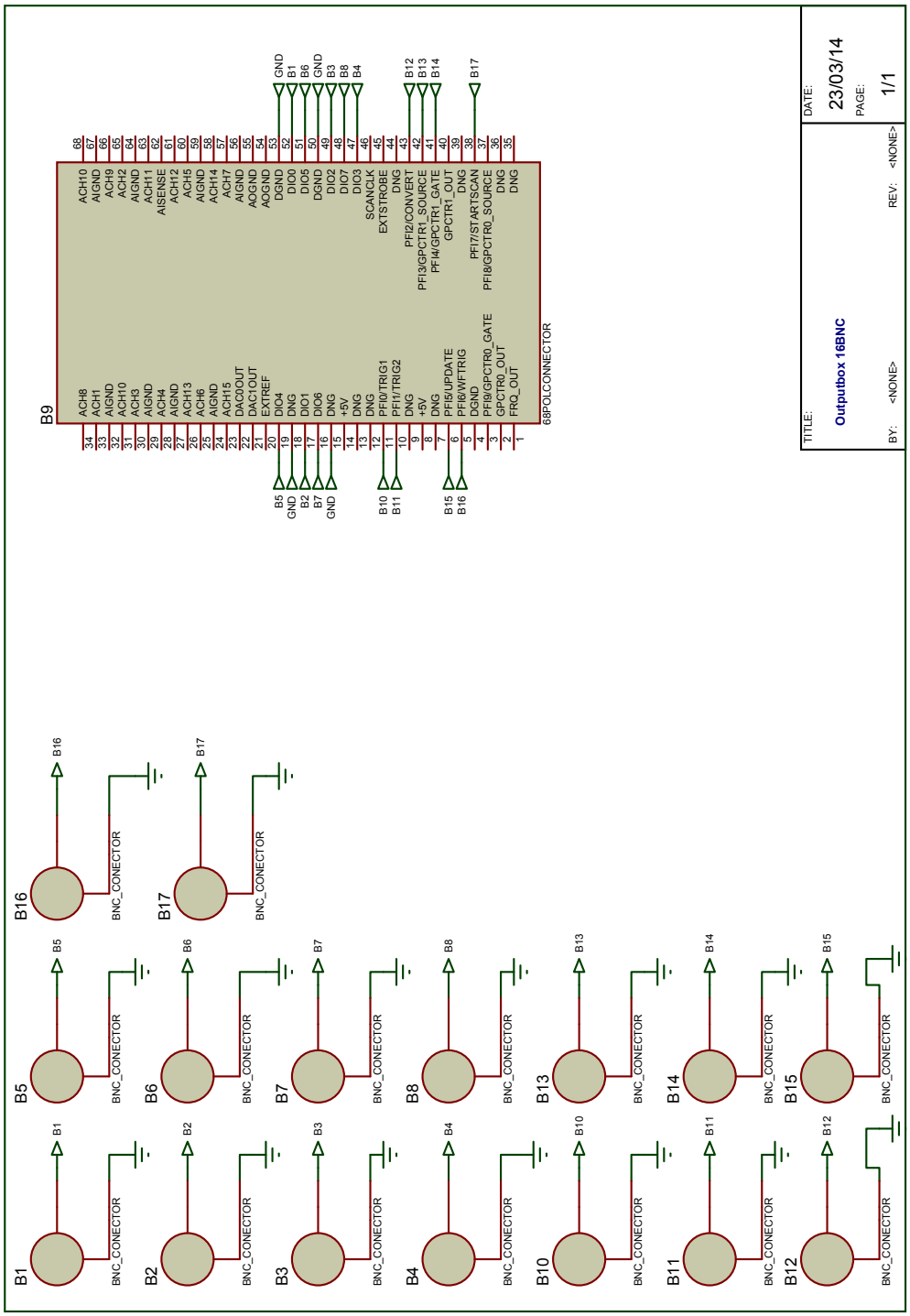

Figure B.2: Schematics of the output-box

C How to build servo motors for your experiment

We want to build some servo motors as shutters for our setups. The servo motors are small nice devices but they are not so easy to control. The communication is shown in figure C.1. The communication is too fast for the normal Labview outputs and we don't work via a counter output because we need them for other applications. In the end we built in a PIC18F2455, this is a microprocessor with an internal USB communication. We used the Usb4all circuits from the internet. If you are interested in Usb4all go to [22].

The Usb4all device has many other features but we actually only use the servo outputs.

- 20 or 31 digital Input/Output Pins (TTL)
- 10 analogue ADC-inputs (0..5V) with 10 or 12 bits resolution
- 1 frequency counter (up to 50 MHz)
- one RS232-interface
- one I2C-Master-interface
- one SPI- interface for up to 6 slave-select-wires
- one microwire- interface
- one shift-register-interface
- interface for 2 LCD-dot-matrix-displays
- 2 PWM-Outputs
- 4 stepper motor interfaces for ABCD-phase-connections
- 4 stepper motor interfaces for L297-circuits
- Connections for 13 model-servos.
- 2 impulse-counter-inputs
- 192 Byte internal EEPROM-memory

PIC-Type	Number of digital IO-Pins	ADC resolution
PIC18F2455 / PIC18F2550	20	10 bit
PIC18F4455 / PIC18F4550	31	10 bit
PIC18F2458 / PIC18F2553	20	12 bit
PIC18F4458 / PIC 18F4553	31	10 bit

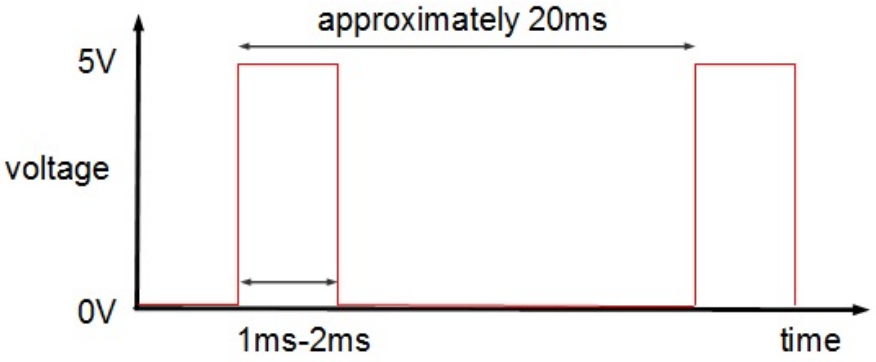

Figure C.1: Pulse width modulation communication with the servo motors. The pulse duration should be 1ms for one endpoint 2ms for the other and a repetition time of approximately 20ms. The repetition time is not defined exactly.

D How to build a MW antenna for NV centres

An MW antenna structure is usually built with a $\frac{\lambda}{2}$ or $\frac{\lambda}{4}$ feature. In the simplest way this is only a metal stick of the right length. See for example [7]. This book explains how to build an antenna which produces photons with an exact defined wavelength and with some optimization algorithms it is possible to built an antenna which emits a lot of power. But for all NV antennas which are used in this thesis this is not needed. To drive the MW transition only a high magnetic field is used which oscillates with the right frequency. All antennas are built as a short to maximise the magnetic field. The diamond is located on top of the antenna. The diamond thickness lies between $50\mu m$ and $200\mu m$. So the distance between the antenna and NV centre is a lot smaller than the wavelength itself.

All antennas are built on circuit boards. That is very useful because a lot of different designs are possible and the repeatability is given every time, differently to an antenna which uses only a wire.

The lines on the board are built as grounded coplanar waveguides and could be calculated with the program Line [6]. The lines are optimised at 50 Ohm. In this case it does not really make much sense because usually the internal resistance and the load resistance are designed to have the same size to maximise the power the output. Our load resistor is a short. That means that there is no resistance. It does not really make much sense to match this. However it works because the diamond is really close to the antenna.

All antennas are built off resonant to create a relatively homogeneous B-field over the entire range of frequencies of interest.

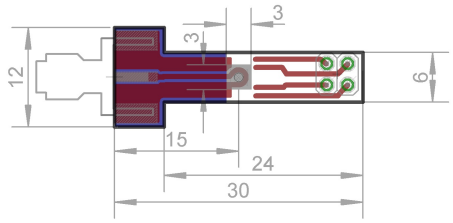

(a) This antenna is used for all experiment in this thesis.

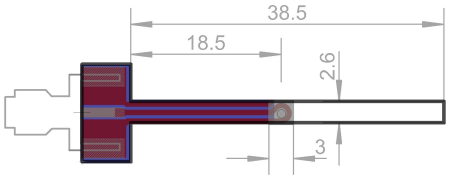

(b) Thin antenna for the cube

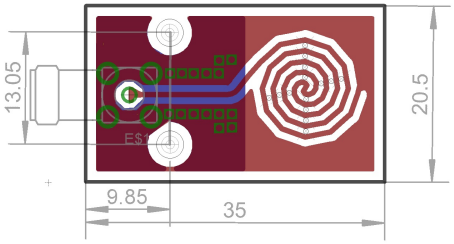

(c) This antenna was built to have an high and homogeneous field at a distance of $200\mu m$ or more over the antenna. This antenna was built for the microscope setup.

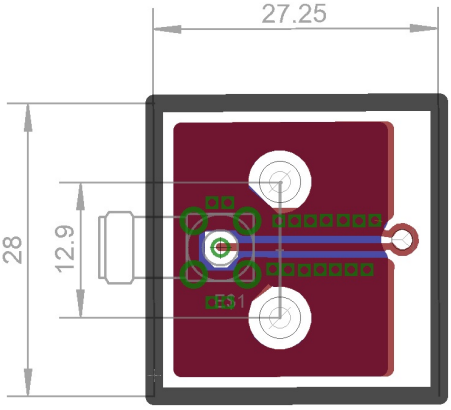

(d) This antenna is an alternative model to the spiral antenna

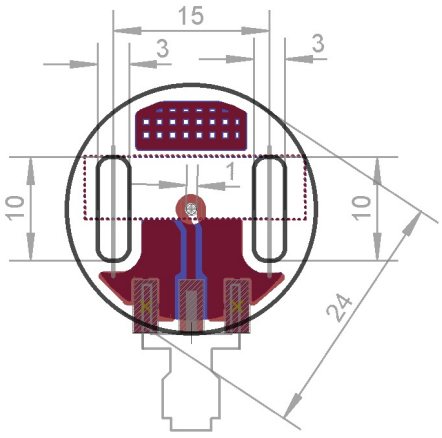

(e) This antenna was built for a cavity setup

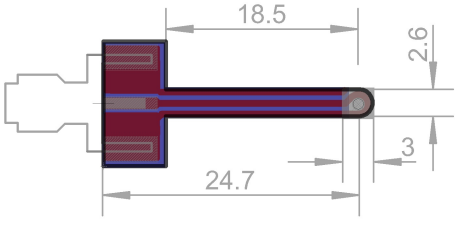

(f) This antenna was built as universal antenna for different types of measurements

Figure D.1

References

[1] Aslam, N., Waldherr, G., Neumann, P., Jelezko, F., Wrachtrup, J., 2013. Photo-induced ionization dynamics of the nitrogen vacancy defect in diamond investigated by single-shot charge state detection. New Journal of Physics 15.

[2] Balasubramanian, G., Neumann, P., Twitchen, D., Markham, M., Kolesov, R., Mizuochi, N., Isoya, J., Achard, J., Beck, J., Tissler, J., Jacques, V., Hemmer, P. R., Jelezko, F., Wrachtrup, J., 2009. Ultralong spin coherence time in isotopically engineered diamond. Nature materials.

[3] Batalov, A., Jacques, V., Kaiser, F., Siyushev, P., Neumann, P., Rogers, L., McMurtrie, R., Manson, N., Jelezko, F., Wrachtrup, J., 2009. Low temperature studies of the excited-state structure of negatively charged nitrogen-vacancy color centers in diamond. Physical Review Letters 102.

[4] Baudenbacher, F., Fong, L. E., Holzer, J. R., Radparvar, M., 2003. Monolithic low-transition-temperature superconducting magnetometers for high resolution imaging magnetic fields of room temperature samples. Applied Physics Letters 82.

[5] Beha, K., Batalov, A., Manson, N. B., Bratschitsch, R., Leitenstorfer, A., 2012. Optimum photoluminescence excitation and recharging cycle of single nitrogen-vacancy centers in ultrapure diamond. Physical Review Letters PRL 109, 097404.

[6] Dellsperger, F., 1998. Line version 1.00. free licence.

[7] Demtröder, W., 2006. Demtöder Experimentalphysik 2 Elektrizität und Optic. Springer Verlag GmbH.

[8] Doherty, M. W., Dolde, F., Fedder, F., Jelezko, H., Wrachtrup, J., Manson, N. B., Hollenberg, L. C. L., 2012. Theory of the ground-state spin of the nv^- center in diamond. Physical Review 205203.

[9] Faley, M. I., Poppe, U., Urban, K., Paulson, D. N., Fagaly, R. L., 2006. A new generation of the hts multilayer dc-squid magnetometers and gmeters. Phys.: Conf. Ser 43 1199.

[10] Gabureac, M., Alvarez, L. S. E., Marrows, C., 2009. Co/pt hall sensors for low field detection. Procedia Chemistry 851854.

[11] Gabureac, M., Bernau, L., Utke, I., Boero, G., 2010. Granular coc nano-hall sensors by focused-beam-induced deposition. Nanotechnology 21 115503.

[12] Haken, H., Wolf., H., 2006. Molekülphysik und Quantenchemie, Einführung in die experimentellen und theoretischen Grundlagen. Springer Verlag GmbH.

[13] ic hause, 2013. ic-hg 3 a laser switch ic hause. http://www.ichaus.com.

[14] Jensen, K., Leefer, N., Jarmola, A., Dumeige, Y., Acosta, V. M., Kehayias, P., Patton, B., Budker, D., 2014. Cavity-enhanced room-temperature magnetometry using absorption by nitrogen-vacancy centers in diamond. arXiv preprint 1401.2438v1.

[15] Kirtley, J. R., Ketchen, M. B., Stawiasz, K. G., Sun, J. Z., Gallagher, W. J., Blanton, S. H., Wind, S. J., 1995. High-resolution scanning squid microscope. Appl. Phys. Lett. 1138.

[16] Liu, G., Li, X., Sun, X., Feng, J., Ye, C., Zhou, X., 2013. Ultralow field nmr spectrometer with an atomic magnetometer near room temperature. Journal of Magnetic Resonance 237, 158163.

[17] Maze, J. R., Stanwix, P. L., Hodges, J. S., Hong, S., Taylor, J. M., Cappellaro, P., Jiang, L., Dutt, M. V. G., Togan, E., Zibrov, A. S., Yacoby, A., Walsworth, R. L., Lukin, M. D., 2008. Nanoscale magnetic sensing with an individual electronic spin in diamond. Nature Letters 455 2.

[18] Onsemi, 2006. And8020 termination of ecl devices with ef (emitter follower) output structure. http://onsemi.com.

[19] Robledo, L., Bernien, H., van der Sarand Ronald Hanson, T., 2011. Spin dynamics in the optical cycle of single nitrogen-vacancy centres in diamond. New Journal of Physics 13.

[20] Scully, M. O., Zubairy, M. S., 1997. Quantum Optic. Cambrige University Press.

[21] Shah, V., Knappe, S., Schwindt, P. D. D., Kitching, J., 2010. Subpicotesla atomic magnetometry witha microfabricated vapour cell. Optics Express 18, 27167–27172.

[22] Sprut, 2012. Usb4all v.10 technical description user manual. http://www.sprut.de.

[23] Tiporlini, V., Alameh, K., 2013. High sensitivity optically pumped quantum magnetometer. The Scientific World Journal.

[24] Vasyukov, D., Anahory, Y., Embon, L., Halbertal, D., Cuppens, J., Neeman, L., Finkler, A., Segev, Y., Myasoedov, Y., Rappaport, M. L., Huber, M. E., Zeldov, E., 2013. Scanning nano-squid with single electron spin sensitivity. Nature Nanotechnology Letter 8,639644.

[25] Zaitsev, A. M., 2001. Optical properties of diamond. Springer Verlag Berlin Heidelberg New York.